# Circulation in the Strait of Juan de Fuca:

## Recent Oceanographic Observations in the Eastern Basin

J. R. Holbrook, R. D. Muench,
D. G. Kachel, and C. Wright

Pacific Marine Environmental Laboratory
Seattle, Washington

**April 1980**

## NOTICE

Mention of a commercial company or product does not constitute
an endorsement by NOAA Environmental Research Laboratories.
Use for publicity or advertising purposes of information from
this publication concerning proprietary products or the tests
of such products is not authorized.

# CONTENTS

# CIRCULATION IN THE STRAIT OF JUAN DE FUCA: RECENT OCEANOGRAPHIC OBSERVATIONS IN THE EASTERN BASIN[1]

### J. R. Holbrook, R. D. Muench,[2] D. G. Kachel, and C. Wright

ABSTRACT. In two field experiments conducted in the eastern Strait of Juan de Fuca during winter 1977-78 and summer 1978, 3-mo time series measurements of currents, over-the-water winds, shore winds, and water properties were obtained. From these data sets, the principal water motions are identified and described. Over time scales of 4 to 25 h, tidal currents dominate the current fluctuations and account for 58% to 99% of the current variance. Mean flow is characterized by an estuarine circulation that consists of a vigorous two-layer pattern with near-surface velocities directed seaward at 20 to 40 cm/s and deep layer velocities directed landward at 10 cm/s. Although local winds play a minor role in modifying near-surface circulation, coastal storms dramatically affect circulation in the eastern basin. During the winter experiment seven current reversals (up-strait subtidal flow) were observed for periods of 2 to 6 days and had eastward maximum velocities of 20 cm/s. The extent to which coastal winds affect flow in the eastern basin depends on their strength, duration, and direction. The reversals that propagated up-strait at speeds of 20 to 30 cm/s were observed as far as New Dungeness Spit, 135 km east of Cape Flattery. Coastal Ocean Dynamics Applications Radar (CODAR) surface drifter and current measurements during an intensive 4-day study period further delineate the spatial characteristics of a single coastally generated reversal. Although the long-term average near-surface flow is seaward, the effects of tidal currents and coastal storms and the resultant complex pattern of eddies, fronts, and shore-directed currents lead to a regime in which surface pollutants could impact the shore as far east as Whidbey Island.

## 1. INTRODUCTION

The Strait of Juan de Fuca is the principal channel connecting the inland waters of Puget Sound and the Strait of Georgia with the North Pacific Ocean. It is the main shipping route to major northwest Canadian and U.S. population centers, and accounts for most of the water exchange between the populous inland waterways and the open ocean. Since these waterways, including the Strait, are used for both industry and recreation, a working knowledge of the marine environment is needed on which to base management decisions.

In 1975 the Pacific Marine Environmental Laboratory (PMEL) of NOAA began studies on several oceanographic aspects of the Strait, emphasizing water circulation. Investigations during the first 2 yr resulted in a comprehensive report (Cannon, 1978) that summarized existing knowledge and discussed results of field work in the western Strait. Our report presents the results of field work in 1977-1978 in the eastern portion of the Strait of Juan de Fuca and synthesizes these results with those presented in Cannon's report. Together these two papers constitute the final report for the program and provide a comprehensive description of oceanographic circulation in the Strait of Juan de Fuca. While emphasizing water movement in the eastern Strait, this report describes net and fluctuating flows, seasonal variability, and driving mechanisms. No attempt is made to relate this work to ecosystem studies.

## 1.1 Physical Oceanography

Estuarine systems are defined as regions where terrestrial runoff and marine waters mix (Pritchard, 1967). They are generally, but not necessarily, stratified in salinity and density. Consequently, maximum vertical density stratification can be expected during periods of large freshwater input, such as spring snowmelt or autumn and winter storms, and minimum stratification occurs during periods of small freshwater input.

The Strait of Juan de Fuca may be considered a weakly stratified, partially mixed estuary with strong tidal currents (100 to 150 cm/s), a 3- to 4-m spring tide height range, and a surface-to-bottom salinity differential of $2^o/_{oo}$ to $3^o/_{oo}$ (Herlinveaux and Tully, 1961; Rattray, 1967). Freshwater runoff primarily enters the Strait of Georgia (via the Fraser River) and Puget Sound where the circulation is a fjord type. Before entering the eastern Strait of Juan de Fuca, these diluted source waters are tidally mixed in the passages leading through the San Juan Archipelago and across Admiralty Inlet. Although there are important cross-channel variations, the along-strait mean flow may be characterized by the classic estuarine circulation with out-strait (westward) transport near the surface and in-strait (eastward) transport near the bottom. This circulation is maintained by fresh water that enters the system and sets up a longitudinal sea-surface slope and internal density gradients.

The significance of low-frequency current fluctuations in estuarine systems has only recently been recognized, aided by the availability of extended time series current observations. Observational studies of these processes in other estuaries have been described by Elliott (1978), Wang (1979), Wang and Elliott (1978), Muench and Heggie (1978), Svendsen (1977), and others. Low-frequency fluctuations in the Strait of Juan de Fuca have been analyzed by Holbrook and Halpern (1977, 1980) and Holbrook et al. (1980). These studies have revealed that the low-frequency fluctuations can be driven either by local winds or by offshore forcing that causes coastal sea level fluctuations. In the deeper, partially mixed estuaries, offshore forcing appears to be dominant.

In addition, descriptive data analyses for the Strait of Juan de Fuca have been presented by Cannon and Laird (1978), Fissel (1976), Fissel and Huggett (1976), Herlinveaux and Tully (1961), Hugget et al. (1976), and Thomson (1975). The scope of these studies has been limited by the availability of data, but they provided useful input for Cannon's 1978 synthesis of oceanographic conditions in the Strait.

## 1.2 Geography

The Strait of Juan de Fuca is a glacially formed submarine valley intruding landward from the Pacific Ocean. At its eastern end it bifurcates to form the channels of the San Juan Archipelago, connecting to the Strait of Georgia to the north, and Admiralty Inlet leading southward to Puget Sound (fig. 1). It is bounded on the south by the 1,800-m-high Olympic Range and to the north by the Seymour Range on Vancouver Island, where elevations reach 1,200 m. An effective 60-m-deep sill projects southward off Victoria and separates the Strait into western and eastern basins where depths exceed 100 m (54 km) (fig. 2). The western basin is approximately 20 km wide and 90 km long. Cross-channel bottom topography is generally U-shaped with center-channel depths gradually increasing seaward from 170 m off Port Angeles to 240 m near the mouth north of Neah Bay. Depths of more than 200 m continue along the axis of Juan de Fuca Canyon, which crosses the entire continental shelf. Bottom topography in the eastern basin is more complex; deep channels separate numerous banks and shoals. The deepest channel exiting the eastern basin runs northward through Haro Strait across a 90-m sill into the Strait of Georgia. Sill depths of 45 and 64 m are found in Rosario Strait and Admiralty Inlet, respectively. Ediz Hook and New Dungeness Spit are major landforms that developed along the southern shore of the Strait as a result of eastward littoral drift of glacial deposits from the Elwha River, 5 nmi west of Port Angeles, and nearby cliffs.

## 1.3 Meteorology

The meteorology of western Washington is influenced by the atmospheric high pressure region that normally overlies the eastern Pacific Ocean with its center at about 30°N, 145°W. Much of the coastal wind field can be attributed to a combination of circulation around this
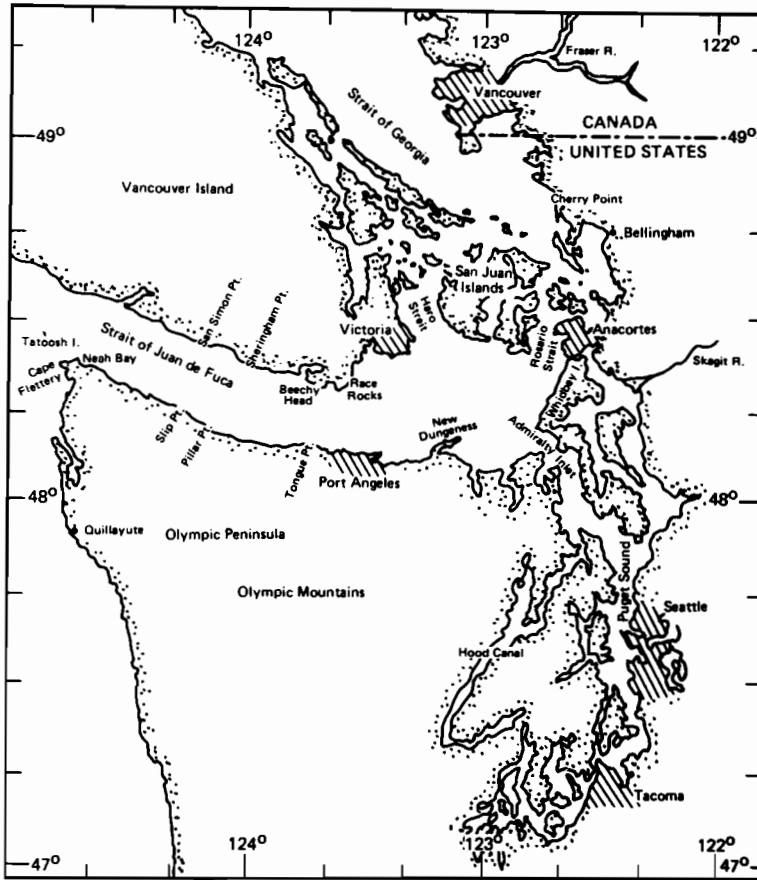
Figure 1.--Strait of Juan de
Fuca, with nearby features
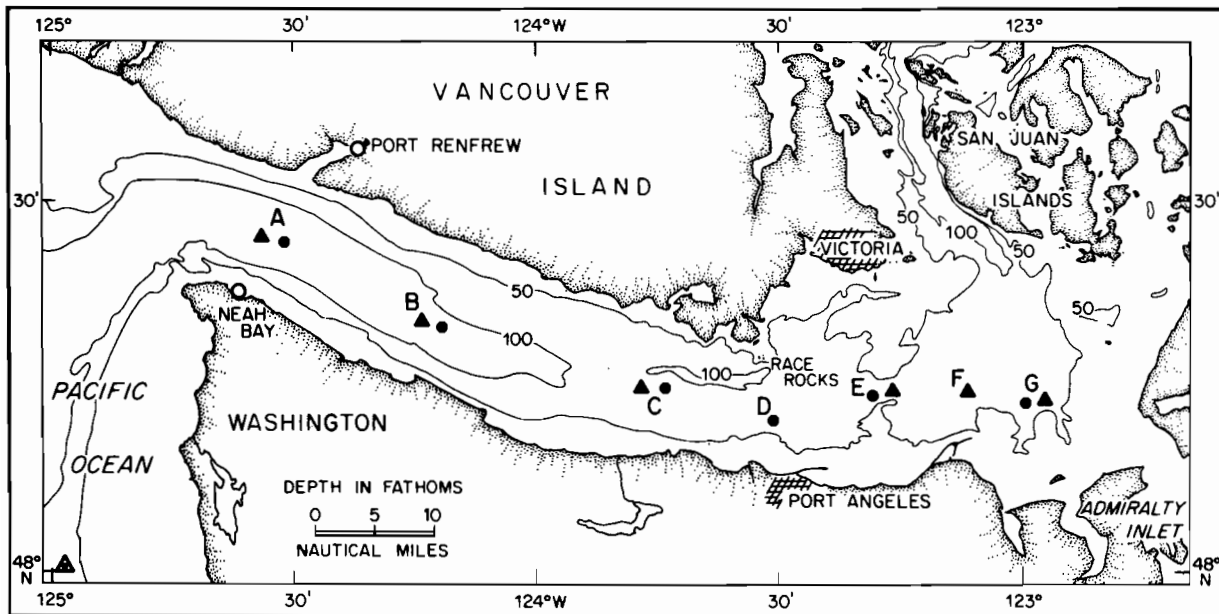and connecting waterways.



Figure 2.--Topography of the Strait of Juan de Fuca. An effective 60-m-deep sill pro-
jects southward from Victoria and separates the Strait into eastern and western basins.
Positions of selected surface (▲) and subsurface (●) current meter mooring sites are
shown. (See also fig.6.) Locations where coastal winds were computed by Bakun (1977)
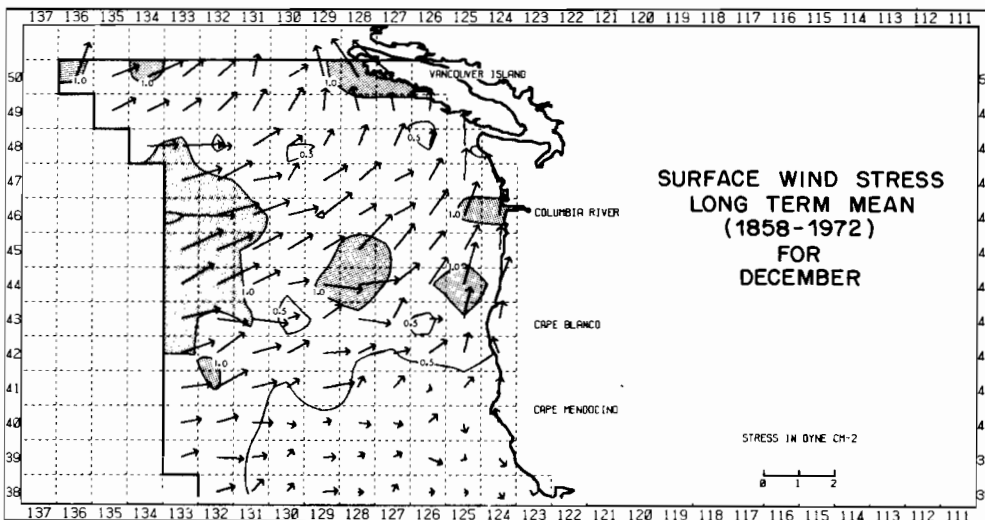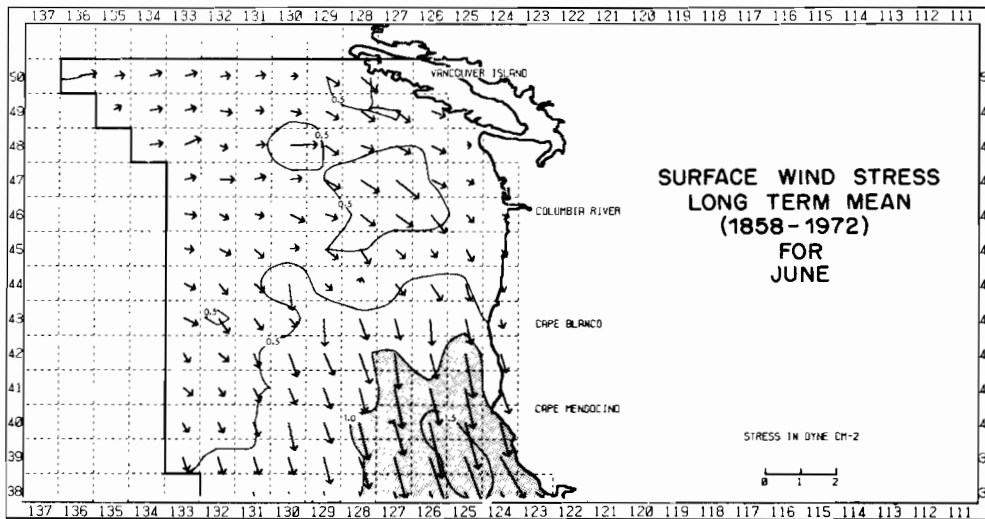are indicated (O).

3

*Figure 3.--Monthly mean (1858-1972) surface wind stress off Washington-Oregon coast during June and December. Values were computed from ship observations. (Adapted from Nelson, 1977.)*

semipermanent high and the passage of migrating low pressure cells. In summer the high is better developed and shifts northward toward the Gulf of Alaska (35°-40°N, 150°W), so that resulting summer winds along the Pacific coast are predominantly northwest. In winter, there is a southward migration and general weakening of the anticyclone. Simultaneously, the semipermanent Aleutian low pressure cell intensifies and causes a reversal of the winds along the Pacific coast. Coastal winds in autumn and early winter are generally southeast, then shift to south-southwest by late winter. Figure 3 shows representative surface wind stress vectors for June and December (Nelson, 1977). These wind stress fields are based on historical surface marine wind observations and illustrate the seasonal variability of the coastal wind field.

Winter weather is dominated by cyclonic storms that migrate across or north of the region and are interspersed occasionally with periods of high pressure. Gale force (17 to 24 m/s) or higher winds occur frequently along the coast near Tatoosh Island. Such gales are southerly, persist for 2 or 3 days, and are accompanied by high sea and swell. From an analysis of 731 weather maps, Maunder (1968) has identified and categorized seven anticyclonic and nine cyclonic weather patterns characteristic of the region. The two most common low pressure pat-

4

terns are those having centers near Vancouver Island and those with centers farther northwest in the Gulf of Alaska. In the first of these patterns, disturbances form in the central Pacific between the Aleutian low and Central Pacific high, traverse the Pacific commonly on an east-northeasterly trajectory, and reach land over Vancouver Island. In the second type, frontal systems spin off from the quasi-stationary low pressure area in the Gulf of Alaska and move rapidly across the Pacific. Such cold fronts frequently stall and dissipate offshore before moving inland. Maunder found that in winter approximately 74% of the patterns could be classified as having low pressure. Occasionally, however, an upper level, high pressure ridge develops over northwest Canada and leads to clear skies, near freezing temperatures, and northeast winds.

Winds over the Strait of Juan de Fuca are strongly influenced by orographic effects. In channels and passageways where continental topography interrupts geostrophic flow of air, winds tend to be directed along-axis from high to low pressure regions. The western Strait of Juan de Fuca is such an orographic channel. For example, when a low pressure system lies off the Washington coast the resultant westward pressure gradient causes westward airflow that accelerates through the Strait with low speeds at Port Angeles and higher speeds at Tatoosh Island. Such an airflow was first described as a "gap wind" by Reed (1931). As storm fronts migrate eastward, the resulting along-strait pressure gradient reverses and generates west winds in the Strait. The unpredictable movement and timing of such frontal systems make forecasting difficult in this region. In general, seaward or easterly winds occur more frequently in winter, whereas landward or westerly winds predominate in summer (Harris and Rattray, 1954).

During summer, northwest coastal winds are funneled up-strait and enhanced by an up-strait atmospheric pressure gradient. More than 75% of all winds at Port Angeles during summer are from the western quadrant. A strong diurnal oscillation or sea breeze, driven by the flow of coastal air that replaces inland air masses that ascend because of daily heating, is superposed on the eastward mean flow.

The three most prevalent regional wind patterns as modeled by Overland et al. (1979) result from (1) an inland high pressure system, (2) a low pressure system passing to the north, and (3) an offshore east Pacific high pressure ridge (fig. 4). The first pattern typi-



INLAND HIGH PRESSURE SYSTEM
(WINTER)



LOW PRESSURE SYSTEM
PASSING TO NORTH
(WINTER)



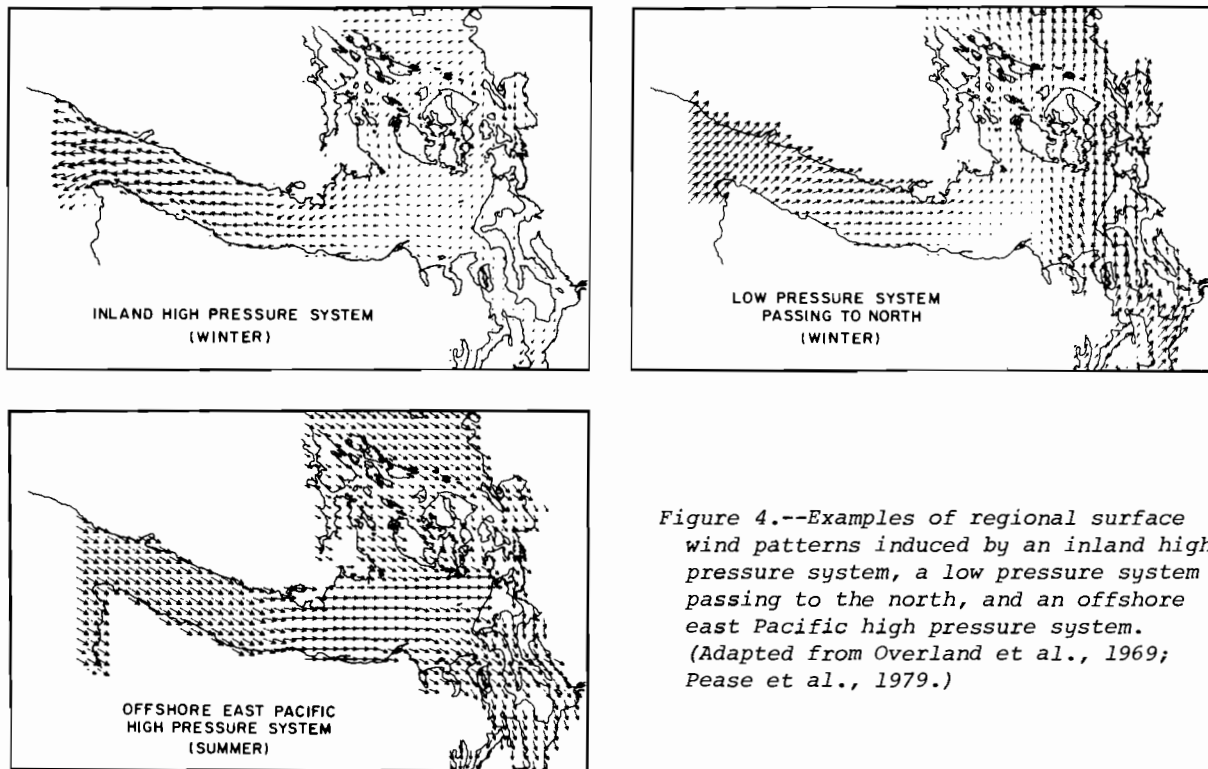OFFSHORE EAST PACIFIC
HIGH PRESSURE SYSTEM
(SUMMER)

*Figure 4.--Examples of regional surface wind patterns induced by an inland high pressure system, a low pressure system passing to the north, and an offshore east Pacific high pressure system. (Adapted from Overland et al., 1969; Pease et al., 1979.)*
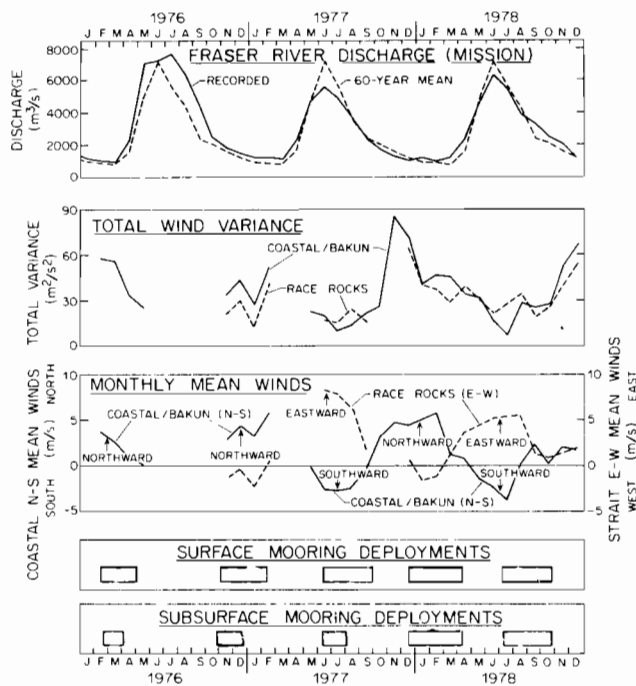
5

Figure 5.--Fraser River discharge, total wind variance, and monthly mean winds during mooring deployments. During winter, discharge was low and wind variance was high with northward coastal winds and variable along-strait winds associated with eastward propagating low pressure systems. During summer, river discharge was high and wind variance was low with southward coastal winds and eastward along-strait winds modulated by a local sea breeze effect.

fies the winds most frequently observed from December through March. Net westward winds increase in strength with distance seaward, particularly in the western Strait. Eastward winds can occur in the Strait year-round during frontal passages, and are caused by the second wind pattern. This pattern accounts for many of the strong westerlies observed during the winter experiment in the eastern Strait. Of interest in this second pattern is the complex wind circulation in the eastern Strait, where southerly winds from Puget Sound converge with westerly winds directed up-strait. Summer months are characterized by persistent westerlies that funnel up-strait and are coherent throughout the length of the Strait. This regional wind situation reflects the third large-scale pressure pattern.

## 1.4 Precipitation and Runoff

Maritime air along the Washington coast is moist and approximately at thermal equilibrium with the ocean surface. During fall and winter, orographic lifting and cooling of inland-moving air masses result in widespread precipitation over the Strait of Juan de Fuca region. The driest section of the region is directly on the northeast side of the Olympic Mountains, and precipitation east of the Olympic Mountains and Vancouver Island is generally much lower than that on the open Pacific coast. The average precipitation at Neah Bay at the entrance of the Strait is 272 cm/yr; at Port Angeles it is 69.5 cm/yr; in the southern San Juan Islands it is 49 cm/yr.

The drainage area into the Strait includes the southern part of the Strait of Georgia (Herlinveaux and Tully, 1961), Puget Sound, and the many smaller seaways. It also includes the San Juan and adjacent islands, the southeastern coastal slopes of Vancouver Island, the coastal slopes of the adjacent mainland, and the Fraser River, which extends inland for about 2,500 km. Most of the terrestrial drainage areas are high mountainous regions, so winter snow storage plays a major part in regulating runoff. The snow cover advances to near sea level in January and retreats to the permanent snow level at about 1,400-m altitude by September. The precipitation is greatest at high altitudes, but drainage does not occur until the spring thaws. Rivers draining the high levels therefore commence to rise in late March and attain maximum discharge in June. This pattern is particularly true for the Fraser River, which supplies up to 70% to 75% of the fresh water discharging into the the Strait (Herlinveaux and Tully, 1961), with the larger proportion probably in June and the smaller in January. During the winter field experiments in the eastern Strait, the Fraser River discharge was near normal; however, peak discharge was below normal in 1977 and 1978 (fig. 5).

6

# 2. CURRENTS IN THE EASTERN STRAIT OF JUAN DE FUCA

## 2.1 Observations and Measurements

Data used to describe circulation processes in the Strait of Juan de Fuca were gathered from remote recording current meters, wind recorders, and tide gages, and shipboard CTD systems. Locations of moored current meters are shown in fig. 6. Table 1 lists depth and period of operation for the meters at each station. Two types of current meters were deployed. Aanderaa RCM-4 current meters were used on taut wire moorings with an anchor and acoustic release at the bottom and a 1,000-lb subsurface buoyancy float above the top current meter (fig. 7). The second type of mooring contained vector-averaging current meters (VACM) suspended below a surface toroidal float (fig. 8); mounted on the buoy tower was a vector-averaging wind recorder (VAWR).

The VACM continuously measures current speed using a Savonius rotor and almost continuously measures direction with a small-vane/vane-follower assembly and magnetic compass. In every 45° of a rotor revolution, a unit vector, with direction computed by adding discrete compass and vane orientations, is internally converted to Cartesian coordinates. These north-south and east-west components are internally summed during the instrument averaging period. The number of data samples or unit vectors used in each vector average is a function of current speed; e.g., a 100-cm/s current would generate approximately 12,000 vector additions over a 7.5-min recording cycle. Such a sampling scheme reduces contamination of the current spectrum by surface wave noise (Halpern and Pillsbury, 1976; Saunders, 1976). Consequently, these meters were considered the most suitable for use on a surface-following mooring subject to wave noise. During data processing, the north-south and east-west sums are converted to current velocity components using calibration formulae given by McCullough (1975). Halpern (1980) has shown that the AMF VACM can yield near-surface current measurements in the open ocean with an accuracy of about 2 cm/s.

The Aanderaa meters, unlike the VACM's, record speed continuously over a preset interval, generally 10, 15, or 20 min, and provide a mean value of speed and an instantaneous direction for each recording interval. They are therefore susceptible to biasing by wave-induced noise from rotor pumping, and were used only below depths of about 30 m on the subsurface moorings.

Data from the Aanderaa meters were resolved into north and east components and low-pass filtered to remove high-frequency noise. Two new data series were then produced using a Lanczos filter (Krancus et al., 1978). The first series was filtered so that more than 99% of the amplitude was passed at periods greater than 5 h, 50% at 2.86 h, and less than 0.5% at 2 h. The second series, filtered to remove most of the tidal energy, passed more than 99% of the amplitude at periods of more than 55 h, 50% at 35 h, and less than 0.5% at 25 h. This series was then resampled at 6-h intervals and used for examining nontidal circulation.

The wind recorders used in this project were mounted on surface buoys (see fig. 8). These VAWR's are modified versions of the VACM operating in an inverted position. In this design wind speed is measured by a Climet three-cup anemometer, and direction is measured by a small balanced vane. These sensors are interfaced to the VACM electronics so that two vector computations are made for each anemometer revolution. Pre- and post-experiment wind tunnel calibrations indicate that wind speeds are accurate to about 0.2 m/s.

Temperature and salinity data were collected by two separate but similar types of CTD systems. A Plessey model 9040, combined with a model 8400 data logger, sampled twice per second for simultaneous values of conductivity, temperature, and depth. Data were recorded during the down cast using a lowering rate of 30 m/min. Nansen bottle samples were taken at each station to assist in temperature and salinity calibration. The data were averaged to provide 1-m mean temperature, salinity, and sigma-t values. In the other CTD system, a Plessey model 9400 coupled with a model 8400 data logger operated with a sampling frequency of 0.2 s. Nansen bottle calibration samples were taken about every third station. Data from both systems were processed in the same manner. Cruises during which CTD data were obtained are summarized in table 2.
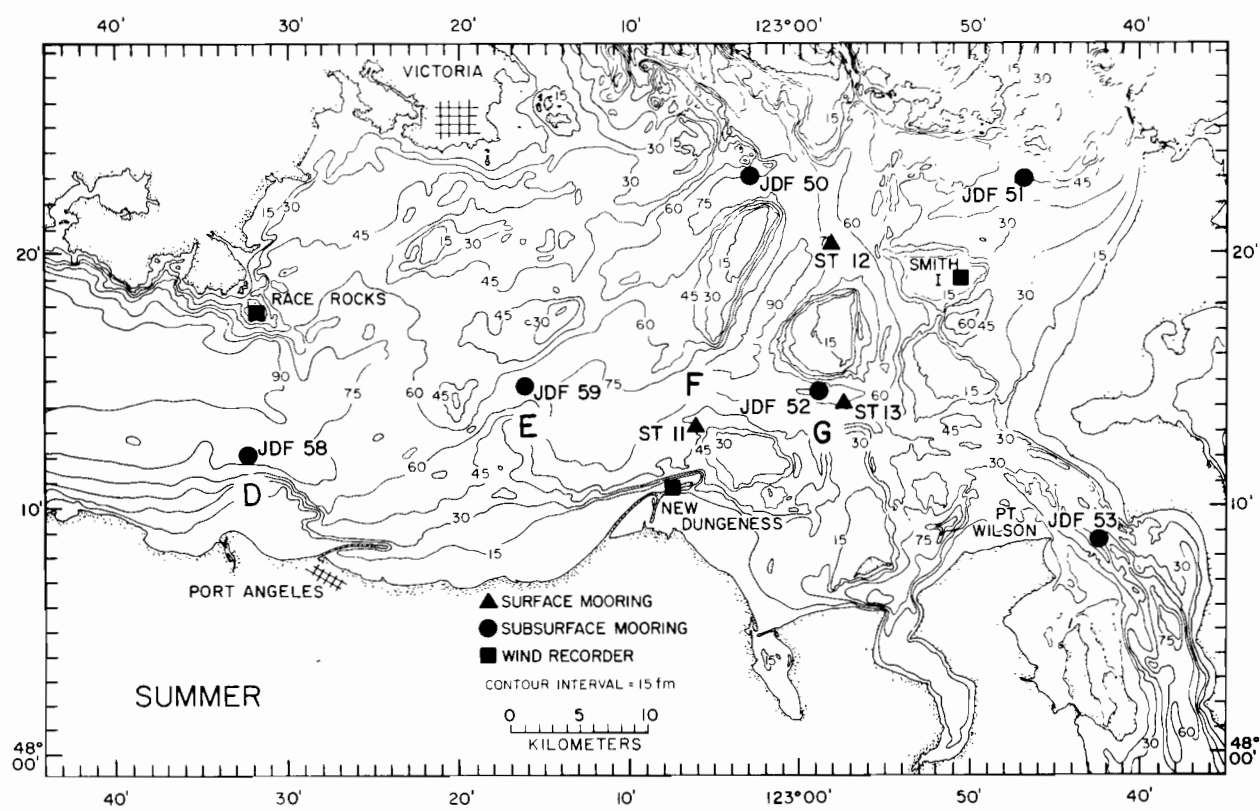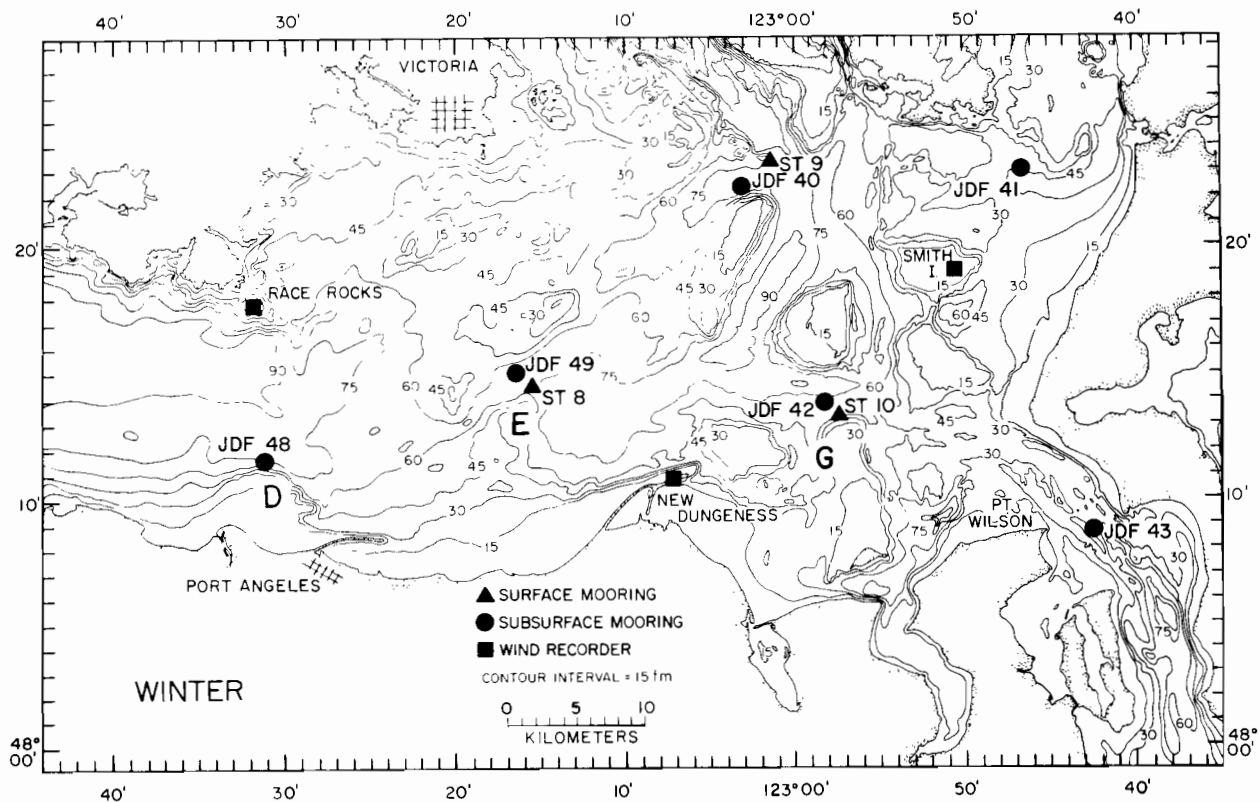
Figure 6.--Positions of surface and subsurface moorings and shore-based wind recorders during winter and summer experiments in the eastern Strait of Juan de Fuca.

8

Table 1.--Summary of mooring deployments

| Mooring | Depth (m) | Recording interval | T (days) | Latitude (N) | Longitude (W) |
|---------|-----------|--------------------|----------|--------------|---------------|
| ST-8 | 4 | 2 Jan 78 - 14 Feb 78 | 44 | 48°14.6' | 123°15.4 |
| | 10 | 2 Jan 78 - 14 Feb 78 | 44 | | |
| | 10 | 19 Dec 77 - 26 Feb 78 | 70 | | |
| | 20 | 19 Dec 77 - 26 Feb 78 | 70 | | |
| | 20 | 19 Dec 77 - 16 Apr 78 | 119 | | |
| ST-9 | 4 | 19 Dec 77 - 6 Apr 78 | 109 | 48°23.3' | 123°01.5' |
| | 4 | 19 Jan 78 - 5 Mar 78 | 46 | | |
| | 10 | 19 Jan 78 - 5 Mar 78 | 46 | | |
| | 4 | 19 Dec 77 - 24 Feb 78 | 68 | | |
| | 20 | 19 Dec 77 - 24 Feb 78 | 68 | | |
| ST-10 | 4 | 19 Dec 77 - 16 Apr 78 | 119 | 48°13.0' | 122°57.2' |
| | 10 | 19 Dec 77 - 16 Apr 78 | 119 | | |
| | 20 | 19 Dec 77 - 5 Mar 78 | 77 | | |
| ST-11 | 4 | 16 Jul 78 - 25 Aug 78 | 41 | 48°14.4' | 123°05.5' |
| | 10 | 16 Jul 78 - 25 Aug 78 | 41 | | |
| | 20 | 16 Jul 78 - 25 Aug 78 | 41 | | |
| | 20 | 16 Jul 78 - 14 Sep 78 | 61 | | |
| ST-12 | 4 | 16 Jul 78 - 23 Aug 78 | 39 | 48°20.6' | 122°56.5' |
| | 10 | 16 Jul 78 - 23 Aug 78 | 39 | | |
| | 20 | 16 Jul 78 - 23 Aug 78 | 39 | | |
| | 4 | 4 Sep 78 - 29 Oct 78 | 56 | | |
| | 20 | 4 Sep 78 - 29 Oct 78 | 56 | | |
| | 20 | 16 Jul 78 - 29 Oct 78 | 106 | | |
| ST-13 | 4 | 16 Jul 78 - 17 Oct 78 | 94 | 48°14.1' | 122°57.4' |
| | 10 | 16 Jul 78 - 17 Oct 78 | 94 | | |
| | 20 | 16 Jul 78 - 17 Oct 78 | 94 | | |
| | 10 | 16 Jul 78 - 29 Oct 78 | 106 | | |
| | 20 | 16 Jul 78 - 29 Oct 78 | 106 | | |
| JDF-40 | 31 | 18 Dec 77 - 3 Feb 78 | 122 | 48°23.3' | 123°03.2' |
| | 61 | 19 Dec 77 - 12 Feb 78 | 56 | | |
| | 131 | 18 Dec 77 - 18 Apr 78 | 122 | | |
| JDF-41 | 29 | 18 Dec 77 - 18 Apr 78 | 122 | 48°23.0' | 122°46.6' |
| | 59 | 18 Dec 77 - 18 Apr 78 | 122 | | |
| JDF-42 | 30 | 18 Dec 77 - 18 Apr 78 | 122 | 48°13.8 | 122°58.3' |
| | 60 | 18 Dec 77 - 18 Apr 78 | 122 | | |
| | 120 | 18 Dec 77 - 18 Apr 78 | 122 | | |
| JDF-43 | 28 | 17 Dec 77 - 26 Mar 78 | 101 | 48°08.7' | 122°42.4' |
| | 43 | 17 Dec 77 - 26 Mar 78 | 100 | | |
| | 68 | 17 Dec 77 - 16 Feb 78 | 63 | | |
| JDF-48 | 23 | 17 Dec 77 - 17 Apr 78 | 123 | 48°11.6' | 123°31.1' |
| | 53 | 17 Dec 77 - 17 Apr 78 | 122 | | |
| | 93 | 17 Dec 77 - 23 Jan 78 | 38 | | |
| | 136 | 17 Dec 77 - 17 Apr 78 | 123 | | |
| JDF-49 | 32 | 17 Dec 77 - 17 Apr 78 | 122 | 48°15.0' | 123°16.5' |
| | 62 | 17 Dec 77 - 17 Apr 78 | 122 | | |
| | 112 | 17 Dec 77 - 12 Jan 78 | 27 | | |
| JDF-51 | 30 | 11 Jul 78 - 3 Oct 78 | 85 | 48°22.9' | 122°46.8' |
| | 60 | 12 Jul 78 - 18 Sep 78 | 69 | | |
| JDF-52 | 30 | 13 Jul 78 - 4 Oct 78 | 84 | 48°14.6' | 122°58.9' |
| | 60 | 13 Jul 78 - 4 Oct 78 | 84 | | |
| JDF-53 | 45 | 11 Jul 78 - 30 Sep 78 | 82 | 48°08.7' | 122°42.3' |
| | 60 | 11 Jul 78 - 20 Sep 78 | 72 | | |

SURFACE

SUBSURFACE FLOAT
26 m

AANDERAA
RCM-4 30m

AANDERAA
RCM-4 50m

AANDERAA
RCM-4 90m

AANDERAA
RCM-4 130m

AMF RELEASE
139m

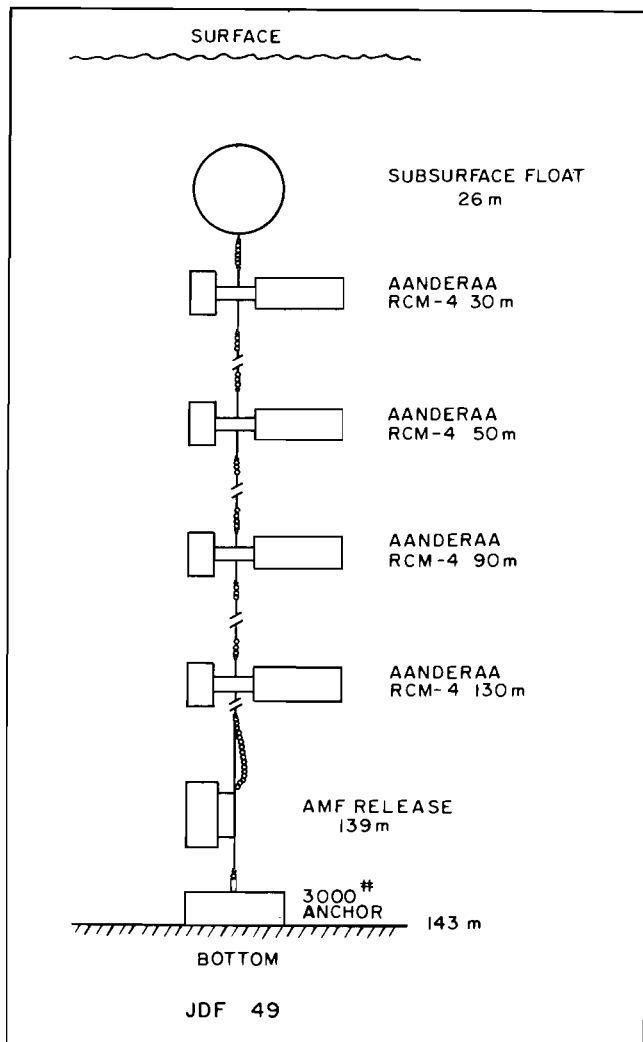3000# ANCHOR    143 m

BOTTOM

JDF 49

Figure 7.--Typical subsurface mooring containing Aanderaa current meters suspended below a 1,000-lb subsurface float.

## 2.2 Energy Distribution

Currents in the Strait of Juan de Fuca were found to be highly time dependent. Current fluctuations were measured over a broad range of time scales, from 15 min to 100 days. Across this band of motions, current energy fell naturally into three principal categories: long-term mean circulation, tidal oscillations, and long-period subtidal fluctuations. The division of fluctuating energy can be seen clearly in representative east-west (solid line) and north-south (dashed line) power density spectra of currents at 4-m depth for mooring sites A and G (fig. 9). Black horizontal bars at the top identify the subtidal (<0.025 cph), diurnal (0.033-0.043 cph), and semidiurnal (0.076-0.085 cph) frequency bands that contained most of the current variance. At 4-m depth, at sites A and G, 86% and 83%, respectively, of the total current variance were contained in these three bands. Table 3 summarizes the variances in other selected current records from the eastern Strait.

The vertical distribution of variance in these bands is illustrated in fig. 10 for sites A and G during winter and summer conditions. Subtidal current variance was greatest near the surface and decreased rapidly with increasing depth in the upper 30 to 40 m of the water column. In the lower layer, subtidal variance represented only a small fraction of total variance. The distribution of tidal variance was more constant with depth and represented most of the total current variance.

Characteristic power density spectra of computed winds off the Washington coast (Bakun, 1977, personal communication) and measured shore winds in the Strait at Race Rocks for winter
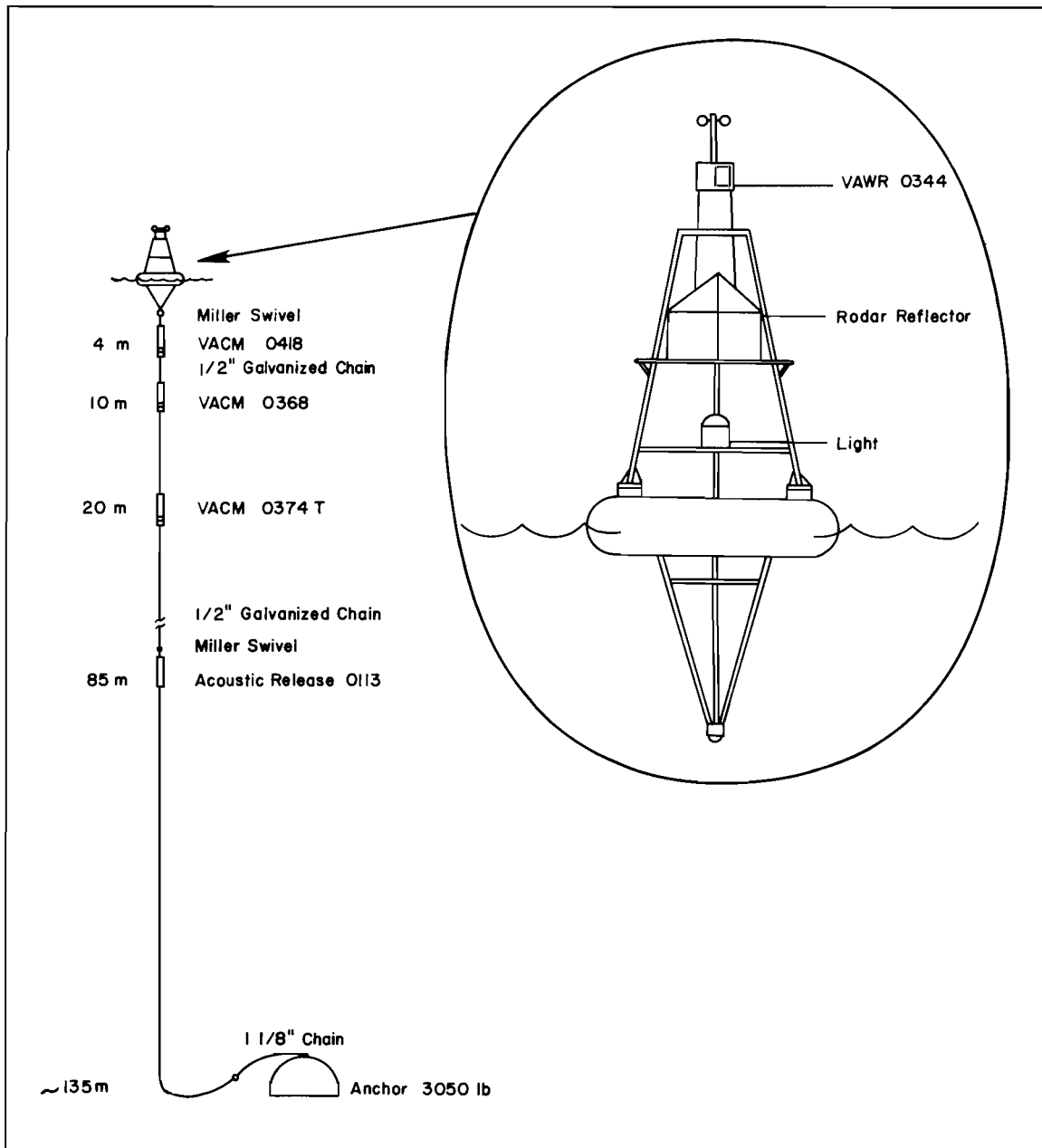
10

Figure 8.--Typical surface mooring containing vector-averaging current meters (VACM's) suspended below a toroidal surface float. Mounted on the surface buoy tower was a vector-averaging wind recorder (VAWR).

and summer conditions are shown in fig. 11. The spectra are red, with 85% to 95% of the variance energy at frequencies below 0.025 cph. At Race Rocks, the total wind variance was nearly the same during winter and summer; however, during winter, it was divided approximately 2:1 between the east-west and north-south components, whereas during summer nearly all the wind variance was contained in the east-west component. Off the coast, wind variance was 88% greater during winter than summer and was divided about equally between components. Although all spectra had an energy peak at time scales of 3 to 6 days, the peak was generally not significant at the 95% level. During summer the east-west components of both coastal and Strait winds had a significant peak at the diurnal frequency, reflecting the influence of the sea breeze effect.

Table 2.--Summary of cruises on which CTD data were collected

| Cruise | Vessel | Dates | No. of stations |
|--------|--------|-------|-----------------|
| OPR509MA76 | MacArthur | 23 Feb - 15 Apr 76 | 141 |
| PR509MA76E | MacArthur | 28-29 Oct 76 | 16 |
| Strait-DI | Discoverer | 3-4 Nov 76 | 33 |
| Snow Goose 1 | Snow Goose | 17-19 Nov 76 | 34 |
| Strait-DI | Discoverer | 15-17 Feb 77 | 39 |
| Strait-DI | Discoverer | 18-21 Jun 77 | 53 |
| Strait-SG | Snow Goose | 19-22 Jul 77 | 65 |
| SG-2 | Snow Goose | 23-26 Aug 77 | 73 |
| Strait-OC | Oceanographer | 22-29 Sep 77 | 163 |
| Strait-OC | Oceanographer | 16-19 Dec 77 | 35 |
| Snow Goose 3 | Snow Goose | 16-20 Dec 77 | 89 |
| Strait-SG | Snow Goose | 12-17 Jan 78 | 133 |
| Strait-DI | Discoverer | 19-21 Mar 78 | 28 |
| Strait-SG | Snow Goose | 11-15 Apr 78 | 48 |
| Strait-SG | Snow Goose | 20-23 Aug 78 | 42 |
| Strait-MC | MacArthur | 31 Oct - 1 Nov 78 | 15 |
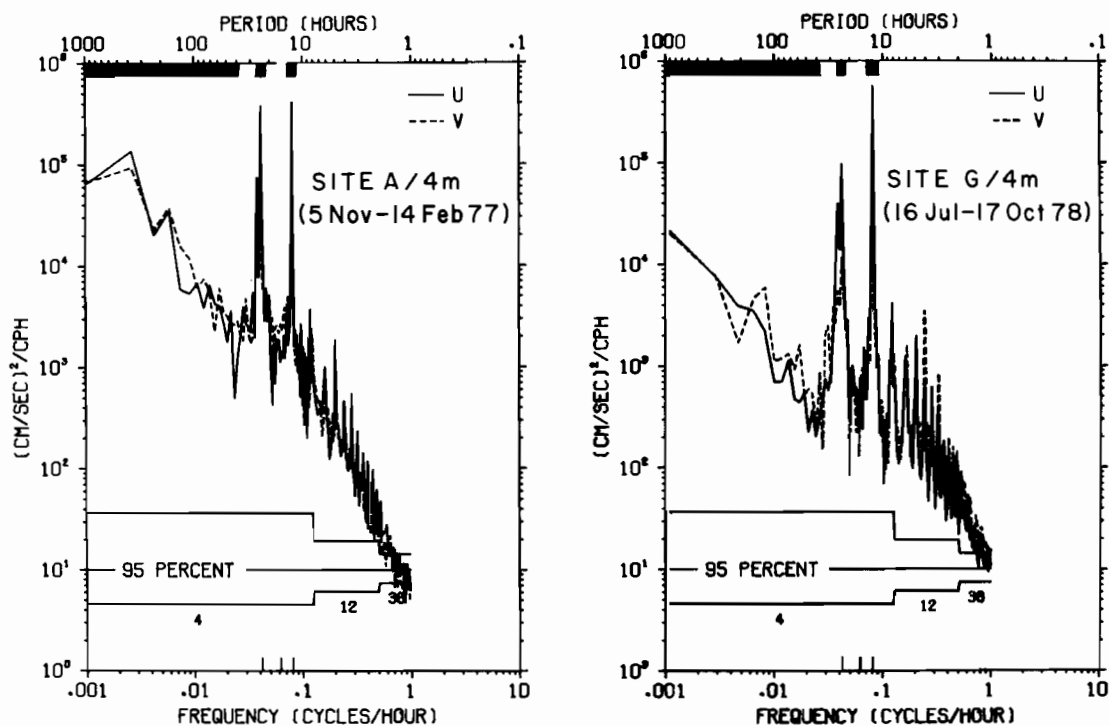


Figure 9.--Density spectra of east-west (U,——) and north-south (V,---) current components at 4-m depth for sites A and G. Black horizontal bars at top identify subtidal (< 0.025 cph), diurnal (0.033-0.043 cph), and semidiurnal (0.076-0.085 cph) frequency bands.

12

Table 3.--Summary of variances in selected current records

| Mooring | Depth (m) | Record length (days) | Total variance (cm²/s²) | | | | |
|---------|-----------|----------------------|-------------------------|---|---|---|---|
| | | | Low-freq. (<0.025 cph) | Diurnal (0.033-0.043 cph) | Semidiurnal (0.076-0.085 cph) | Remainder | Total |
| ST-8 | 4 | 44 | 109 | 725 | 2124 | 185 | 3143 |
| | 10 | 70 | 105 | 694 | 1954 | 251 | 3004 |
| | 20 | 119 | 61 | 510 | 1882 | 181 | 2634 |
| ST-9 | 4 | 109 | 114 | 334 | 691 | 269 | 1408 |
| | 10 | 46 | 101 | 300 | 738 | 139 | 1278 |
| | 20 | 68 | 101 | 369 | 688 | 181 | 1339 |
| ST-10 | 4 | 119 | 158 | 236 | 1070 | 307 | 1771 |
| | 10 | 119 | 112 | 226 | 1054 | 223 | 1615 |
| | 20 | 77 | 75 | 248 | 873 | 146 | 1342 |
| ST-11 | 4 | 41 | 134 | 576 | 1452 | 467 | 2629 |
| | 10 | 41 | 88 | 537 | 1545 | 441 | 2611 |
| | 20 | 41 | 54 | 440 | 1474 | 293 | 2261 |
| ST-12 | 4 | 39 | 63 | 223 | 1642 | 256 | 2184 |
| | 10 | 39 | 55 | 232 | 1562 | 225 | 2074 |
| | 20 | 106 | 41 | 153 | 1124 | 183 | 1501 |
| ST-13 | 4 | 94 | 160 | 353 | 1381 | 577 | 2212 |
| | 10 | 94 | 95 | 318 | 1331 | 269 | 2013 |
| | 20 | 94 | 45 | 268 | 1209 | 186 | 1708 |
| JDF-40 | 31 | 46 | 43 | 443 | 680 | 66 | 1232 |
| | 61 | 55 | 26 | 581 | 665 | 57 | 1329 |
| | 131 | 120 | 64 | 285 | 621 | 161 | 1131 |
| JDF-41 | 29 | 121 | 27 | 267 | 540 | 145 | 979 |
| | 59 | 121 | 28 | 225 | 639 | 106 | 998 |
| JDF-42 | 30 | 121 | 28 | 208 | 698 | 50 | 984 |
| | 60 | 121 | 19 | 207 | 666 | 47 | 939 |
| | 120 | 121 | 19 | 219 | 607 | 104 | 949 |
| JDF-43 | 43 | 98 | 67 | 1863 | 9718 | 265 | 11913 |
| | 68 | 60 | 191 | 1231 | 3633 | 374 | 8795 |
| JDF-48 | 23 | 121 | 155 | 993 | 2504 | 155 | 3807 |
| | 53 | 121 | 44 | 1005 | 3012 | 77 | 4138 |
| | 93 | 36 | 29 | 1626 | 2887 | 72 | 4614 |
| | 136 | 121 | 30 | 814 | 1825 | 213 | 2882 |
| JDF-49 | 32 | 121 | 23 | 763 | 2720 | 11 | 3517 |
| | 62 | 121 | 18 | 690 | 2495 | 69 | 3272 |
| | 112 | 26 | 92 | 422 | 1052 | 498 | 2064 |

13
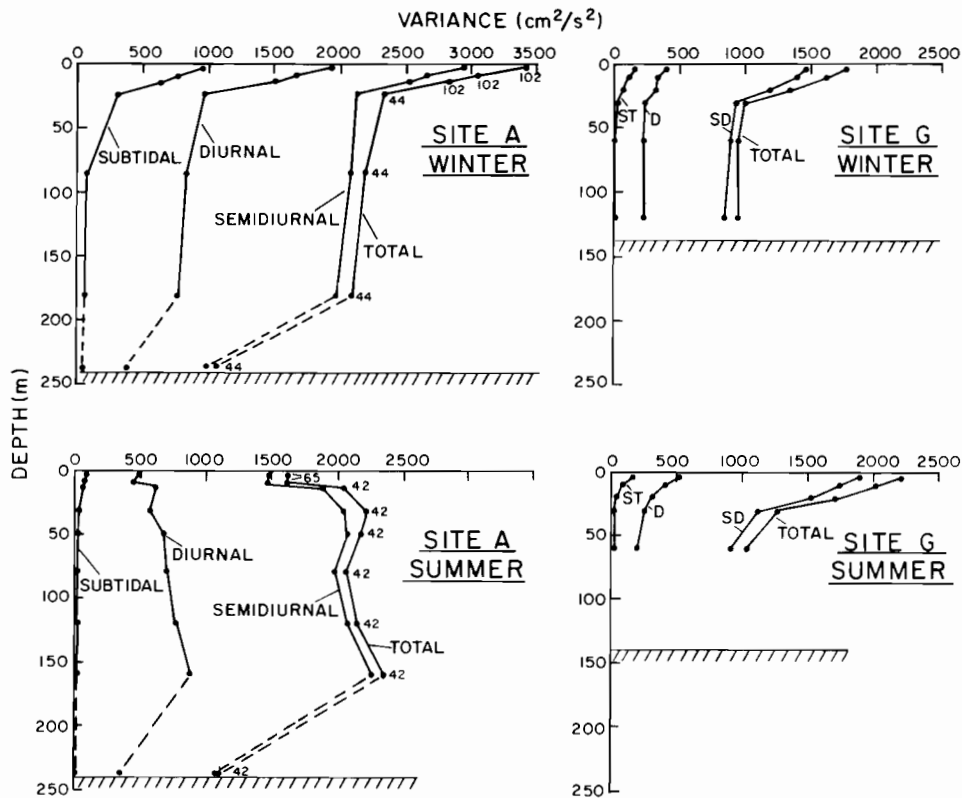
Figure 10.--Vertical distribution of variance in subtidal, diurnal, and semidiurnal frequency bands at sites A and G during winter and summer conditions.

## 2.3 Mean Flow

Mean flow in the eastern Strait of Juan de Fuca is driven by several forces:

- The pressure gradient field maintained by freshwater input from continental runoff, resulting in seaward flow in the upper layer and landward flow in the deep layer. This results in the classic two-layer estuarine circulation.

- Nonlinear interaction of tidal currents with local bottom and lateral topography such that, at the completion of a tidal cycle, a residual flow has occurred.

- Wind stress in a given direction over a period of time, resulting in net wind-driven flow.

The observed total mean flow reflects interaction of these separate modes. Cannon (1978) showed that the two-layer estuarine flow component constitutes a significant portion of total mean circulation in the western Strait of Juan de Fuca.

Observations from current meters at 4-, 10-, 20- and 30-m depths at moorings 49, 40, and 42 (winter) and mooring 52 (summer) indicate that motions in the upper 30 m were vertically highly coherent. Therefore the 30-m records are assumed to represent upper layer flow and are used in the following discussion of flow patterns. It must be noted that net speeds rapidly decreased with depth in the upper layer as a result of the vertical shear maintained by the density field. Table 4 lists vector mean speeds and directions from those moorings in the upper layer where vertical comparison between records was possible. Vertical profiles of net currents near the Strait entrance at site A and in the eastern Strait at site G illustrate the strong two-layer estuarine flow throughout the system (fig. 12).
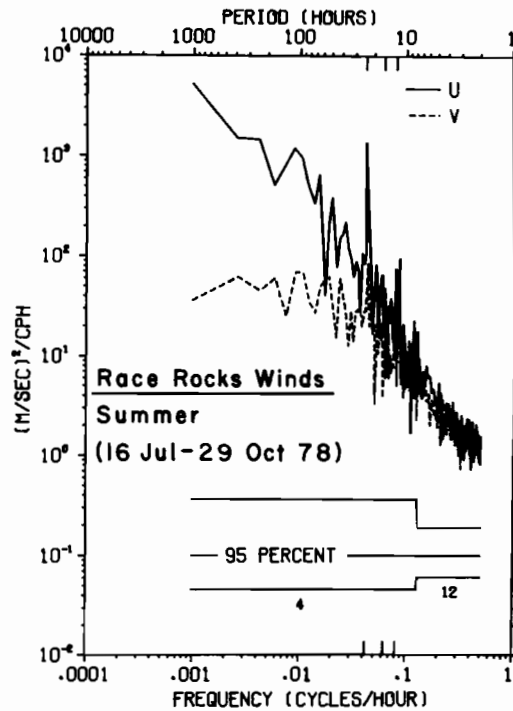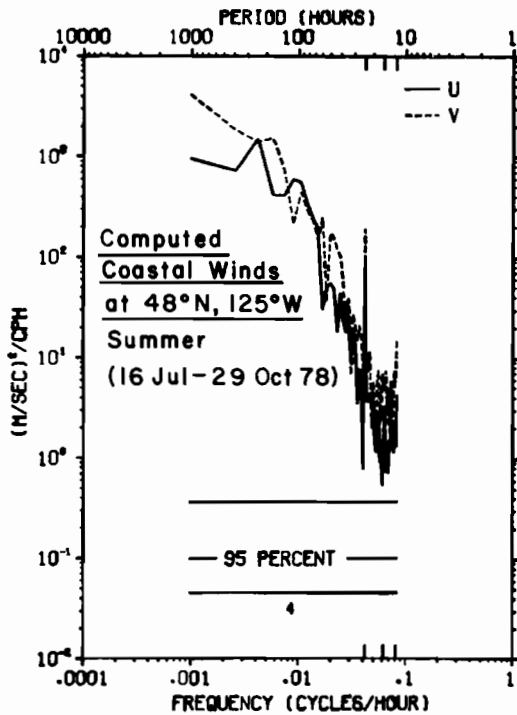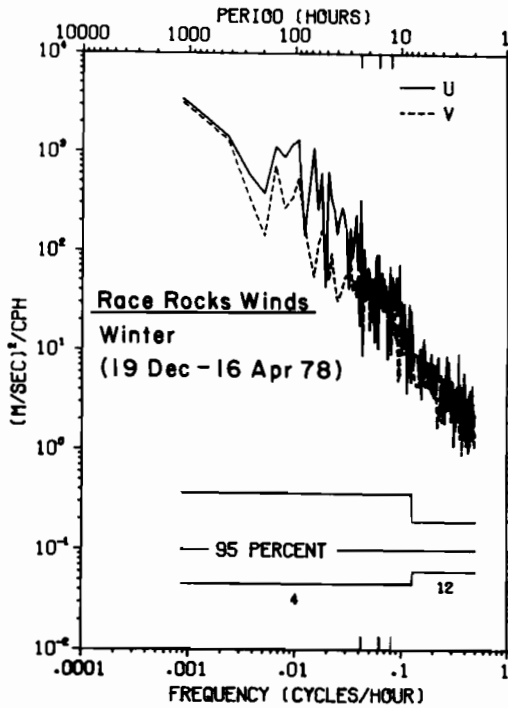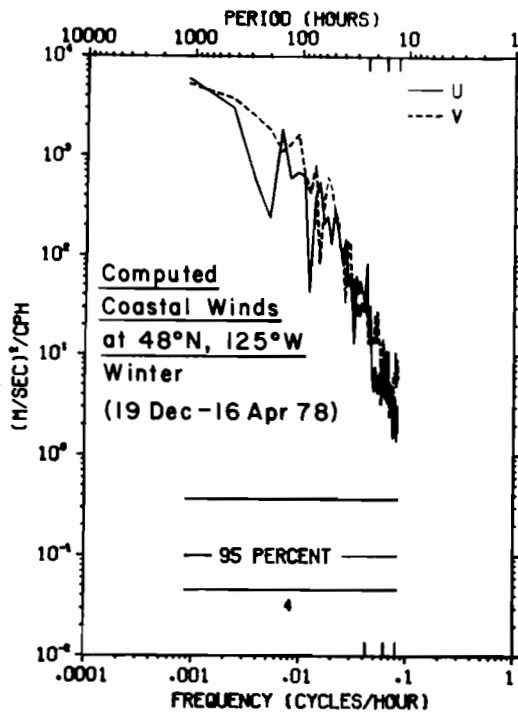
14

Figure 11.--Density spectra of east-west (U,——) and north-south (V,---) wind spectra at 48°N, 125°W, computed by Bakun (1977) and at Race Rocks during winter and summer conditions.

*Table 4.--Vector mean speed and direction for currents in near-surface layer*

| Mooring | Depth (m) | Recording interval | Record length (days) | Latitude (N) | Longitude (W) | Vector mean Speed (cm/s) | Dir.(°T) |
|---------|-----------|--------------------|----------------------|--------------|---------------|--------------------------|----------|
| ST-9 | 4 | 12/19/77 - 4/ 6/78 | 109 | 48°23.3' | 123°01.5' | 15.3 | 324 |
| | 10 | 1/19/78 - 3/ 5/78 | 46 | | | 14.4 | 329 |
| | 20 | 12/19/77 - 2/24/78 | 68 | | | 13.4 | 331 |
| JDF-40 | 31 | 12/18/77 - 2/ 3/78 | 47 | 48°23.2' | 123°03.2' | 7.9 | 013 |
| ST-8 | 4 | 1/ 2/78 - 2/14/78 | 44 | 48°14.6' | 123°15.4' | 20.1 | 243 |
| | 10 | 12/19/77 - 2/26/78 | 70 | | | 19.9 | 251 |
| | 20 | 12/19/77 - 4/16/78 | 119 | | | 19.1 | 246 |
| JDF-49 | 32 | 12/17/77 - 4/17/78 | 122 | 48°15.0' | 123°16.5' | 12.5 | 240 |
| ST-10 | 4 | 12/19/77 - 4/16/78 | 119 | 48°13.0' | 122°57.2' | 22.1 | 319 |
| | 10 | 12/19/77 - 4/16/78 | 119 | | | 19.4 | 317 |
| | 20 | 12/19/77 - 3/ 5/78 | 77 | | | 12.5 | 315 |
| JDF-42 | 30 | 12/18/77 - 4/18/78 | 122 | 48°13.8' | 122°58.3' | 2.1 | 309 |
| ST-13 | 4 | 7/16/78 - 10/17/78 | 94 | 48°14.1' | 122°57.4' | 26.7 | 296 |
| | 10 | 7/16/78 - 10/29/78 | 106 | | | 25.8 | 295 |
| | 20 | 7/16/78 - 10/29/78 | 106 | | | 19.9 | 299 |
| JDF-52 | 30 | 7/13/78 - 10/ 4/78 | 84 | 48°14.6' | 122°58.9' | 6.4 | 298 |

The flow during winter is illustrated by 35-h filtered currents (figs. 13-15) that show upper (30-m) and lower (130-m) layer flow was well developed along the axis of the eastern Strait, particularly at moorings 48, 49, and 42. Numbers around roses indicate percent of observations in that direction, and the length indicates the mean. At moorings 48 and 49, upper layer flow was seaward 60% to 70% of the time at about 15 cm/s. At mooring 42 to the east the seaward flow tendency had decreased to about 50% of the observations, and speeds had slowed to about 5 cm/s. The mid-depth (60-m) records at these three moorings showed a confused pattern because the level of no net flow was near that depth. Consequently, the 60-m mean speeds were smaller than those nearer the surface at moorings 48 and 49 (5-10 cm/s) and also showed a southerly cross-channel trend not present in the upper layer. At mooring 42 the 10 to 15 cm/s mean flow at 60 m was primarily landward (eastward) rather than seaward. Apparently the depth of no net flow was shallower than 60 m at that mooring, whereas it was deeper than or near that depth at moorings 48 and 49. The 130-m depth records indicated landward flow. Mean speeds were about 5 cm/s at mooring 48 and were greater (20 cm/s) to the east at mooring 49. At mooring 42, mean speeds were about 10 cm/s. The record from 48, the westernmost mooring, showed the most directional scatter. From these observations we conclude that the central eastern Strait of Juan de Fuca was characterized during winter by a two-layer mean flow regime with a level of no net motion at about 50 m, which became slightly shallower toward the east.
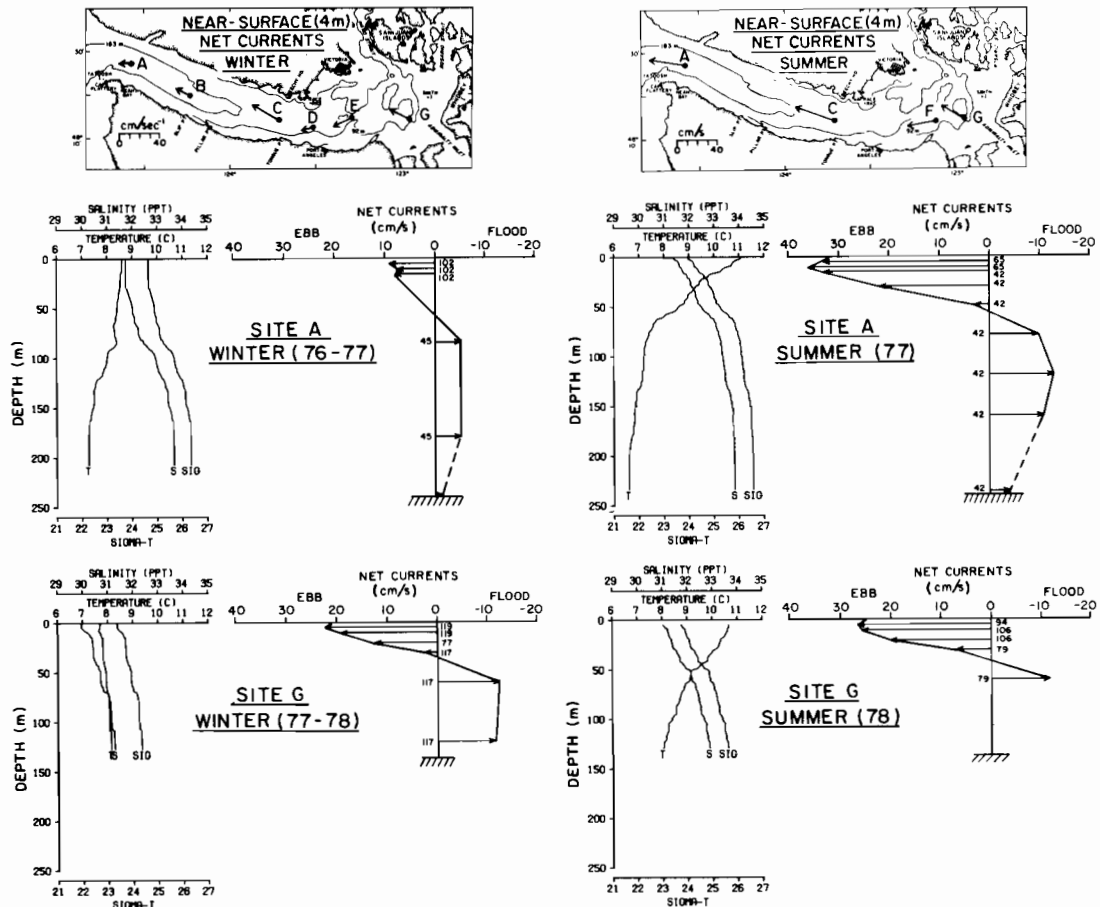
Figure 12.--Vertical distribution of mean along-strait currents and density at sites A and G during winter and summer conditions. Near-shore mean currents at 4-m depth measured from surface moorings are shown at top.

Moorings 40 and 41, situated off the entrances to Haro and Rosario Straits, respectively, showed the influence of flow through those channels. Flow at mooring 40 was northward into Haro Strait at 30 m and had mean speeds of about 10 cm/s. At 60 and 130 m, flow was more variable and had a marked easterly rather than northerly component. Mean speeds at 60 m were about 5 cm/s, whereas at 130 m mean speeds were about 10 cm/s or comparable to the upper layer values. The observations from mooring 41 off Rosario Strait indicated a weak (5 cm/s) southerly flow in the upper layer and a great deal of directional variability. The 60-m record indicated a primarily eastward flow at about 10 cm/s. The flow patterns at these two locations were markedly different from those observed farther south along the axis at the Strait of Juan de Fuca. The two-layer flow regime was not well defined, and, presumably, the circulation in this region is more complicated because of large-scale eddies, bottom topography, and residual tidal flows. The horizontal mooring spacing was not sufficient to resolve large-scale features, and therefore the details of circulation in the northern portion of the eastern Strait are unknown at this time.

The northerly upper layer flow just off Haro Strait was unexpected since freshwater input from sources to the north (the Fraser River) should drive a mean two-layer circulation in Haro Strait. Recent current measurements by Canadian investigators show a well developed two-layer circulation with out-strait flow near the surface in Haro Strait (Webster, 1977). Southerly upper layer flow off Rosario Strait, however, agreed qualitatively with such a pattern. We hypothesize that northward flow into Haro Strait at the mooring sites reflects a tidally driven residual flow caused by flood (northward) tidal currents (see section 2.4). These measurements illustrate that local effects near the mouths of connecting straits may cause complex and often confusing circulation patterns.
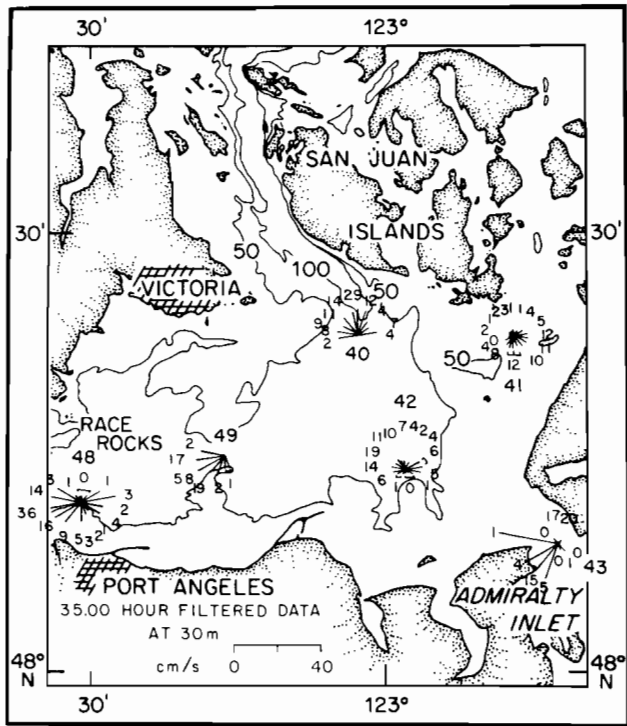
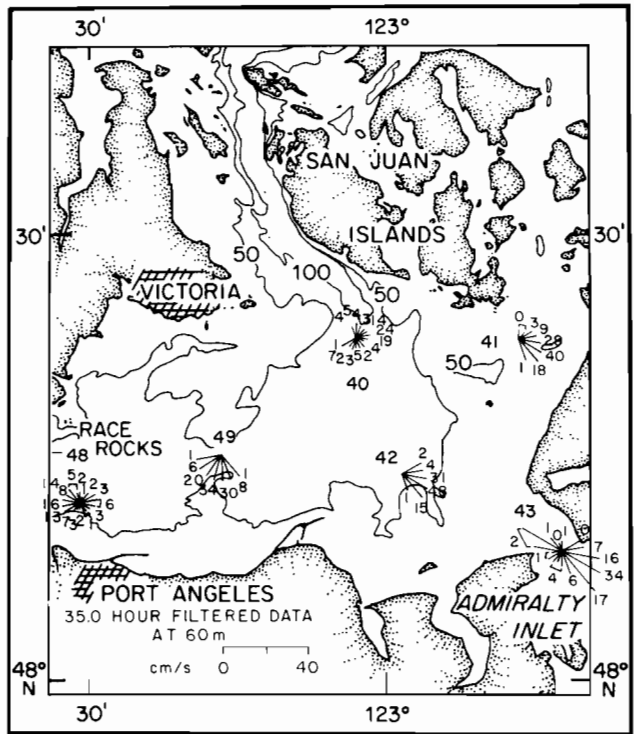Figure 13.--Current roses for 35-h filtered data at 30-m depth during winter.



Figure 14.--Current roses for 35-h filtered data at 60-m depth during winter.
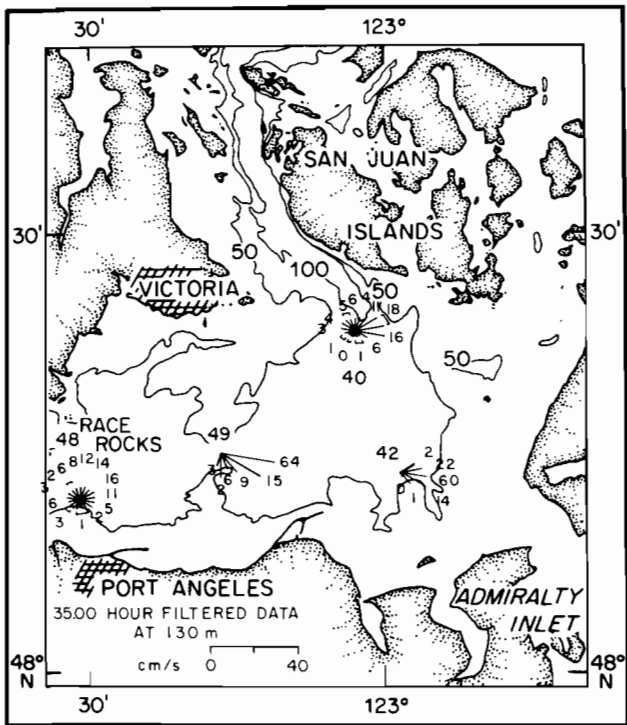


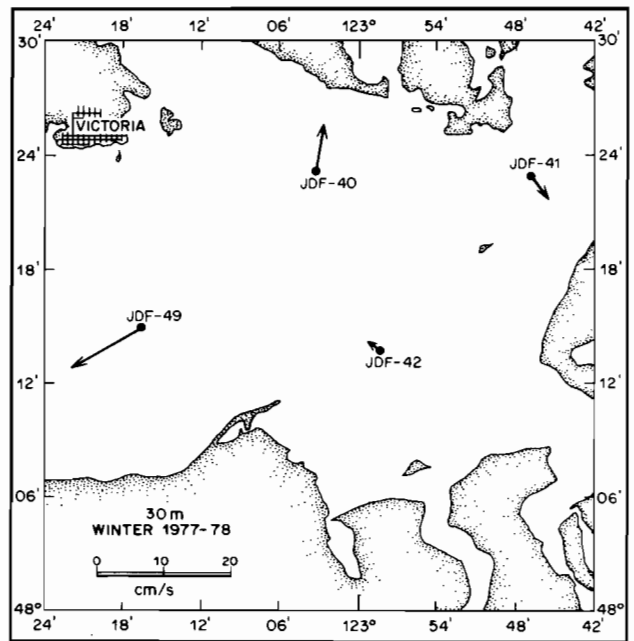Figure 15.--Current roses for 35-h filtered data at 130-m depth during winter.



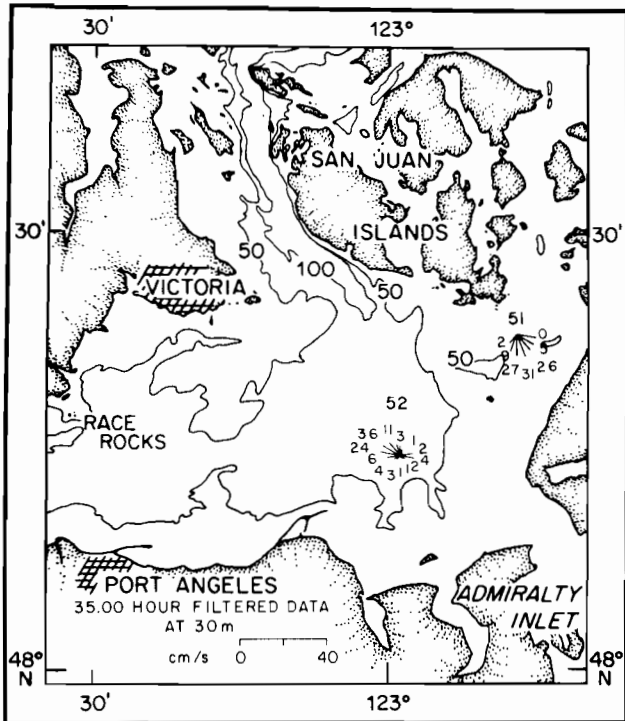Figure 16.--Record-averaged currents at 30-m depth during winter.

18

Figure 17.--Current roses for 35-h filtered
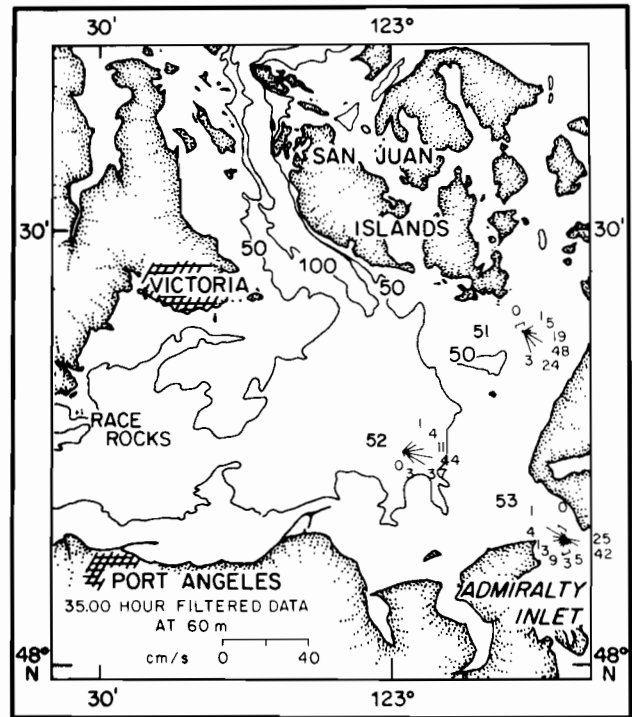data at 30-m depth during summer.



Figure 18.--Current roses for 35-h filtered
data at 60-m depth during summer.

The tendency for mid-depth and deep currents to have easterly or cross-channel flow components was apparently due to a clockwise circulation cell in the eastern Strait, particularly well shown at 30 m during winter 1977-78 (fig. 16). This rotational flow tendency was present at moorings 42, 40, and 41 throughout the water column, and also during the summer at stations 50 and 51 (see current roses in figs. 17 and 18); no data were obtained from station 52. The constancy of this pattern with depth and season suggests that it may be driven by the tides, a mechanism that would tend to force a barotropic, seasonally independent flow. The regional topography is such that ebbing tidal currents from Rosario Strait would tend to form a strait-wide clockwise eddy in the eastern Strait, which might be further abetted by ebb tides from Admiralty Inlet. This eddy would tend to disintegrate during flood tides, but the net effect over several tidal cycles would be a mean clockwise circulation. A test of this hypothesis awaits further analyses of the tidal model developed by Crean (1978).

Currents at the single mooring in Admiralty Inlet, mooring 43, were heavily influenced by the waters of the Puget Sound system to the south (figs. 13, 14, and 18). Strong cross-channel flow at 30 m reflected local topographic influences, whereas a 20 cm/s inward flow at 60 m reflected the estuarine flow regime driven by freshwater input into the Puget Sound system. Because of high peak current speeds (2 to 3 m/s) encountered during ebb and flood tides in Admiralty Inlet, the mooring was subject to considerable drag and consequent heeling. Therefore the middle and upper layer observations are probably not as reliable as the deep layer observations. The upper layer record, moreover, was shorter than the deep layer record because of upper current meter malfunction. Continuity arguments dictate that mean upper and lower layer transports should be similiar since net precipitation (including runoff) minus evaporation was much smaller by comparison. Thus, a mean outflow would be expected in the upper layer, but none was apparent from our records.

Summer current records from the eastern Strait of Juan de Fuca were far less complete than the winter records because of instrument malfunctions and gill net fouling. The 35-h filtered current roses constructed from available summer data indicate the same qualitative flow patterns at 30 and 60 m in the eastern Strait as observed during winter (figs. 17 and 18). There was no statistical difference between winter and summer current speeds. This contrasted
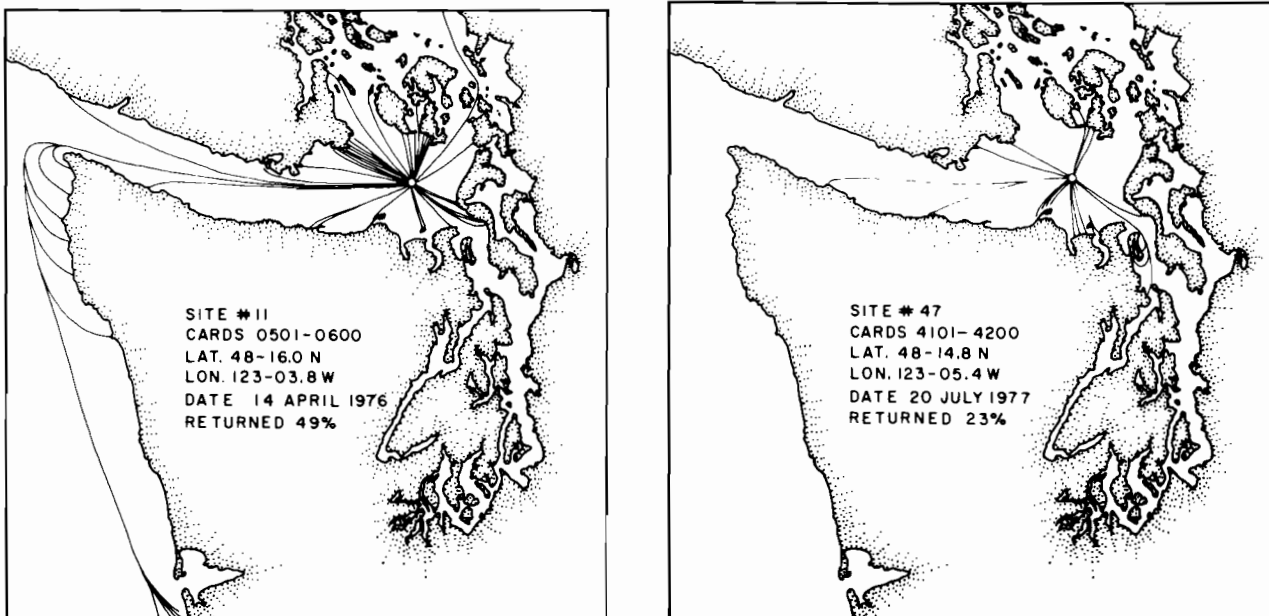
19

*Figure 19.--Examples of drift card recoveries for cards deployed in the eastern Strait (from Pashinski and Charnell, 1979).*

with the western extreme of the Strait where the mean two-layer flow showed summer speeds about double the winter speeds (Holbrook et al., 1979), a result of coastal forcing (see section 2.5.4).

Further evidence for minimal seasonal variation in surface flow in the eastern Strait is provided by results of a drift card study conducted in 1976 and 1977 (Pashinski and Charnell, 1979). These results are in agreement with basic estuarine circulation in the Puget Sound-Strait of Juan de Fuca system as defined by our current observations. The cards released in the eastern basin show the greatest dispersion and on the average were in the water for 3 days or longer before going aground (see fig. 19). However, since winds are the dominant factor in distribution, most cards can be grounded in a short time by very strong winds. Therefore, effective prediction depends on knowing forcing factors in near-real time.

The two-layer estuarine flow is driven by freshwater input, which is reflected in the salinity distribution. Salinities and temperatures recorded during CTD cruises in February, April, October, and November 1976, and in December 1977, were examined for along-strait variations. A consistent change in the horizontal salinity and temperature fields occurred near the sill zone south of Victoria. Separate averages were made for the water masses lying east and west of this natural division.

Most average salinity values in the east were lower than those in the west. Two exceptions were February 1976 and December 1977, when water in the top 100 m in the western Strait had a lower average salinity than water at comparable depths in the eastern Strait. Salinity in the water column increased from top to bottom throughout the system. Surface-to-bottom differences in average values were smaller in the eastern Strait than in the western Strait. For example, in December 1977, the average value in the western Strait was $5.0^\circ/_{oo}$, whereas in the eastern Strait it was $1.8^\circ/_{oo}$.

Horizontal variations in temperature from west to east were typically 1° to 2°C. In the eastern Strait the lowest average temperatures occurred in February and increased throughout the year to December when the highest values were reached. As might be expected, temperature decreased from top to bottom, but even this variation was minimal. In December and February, the differences in temperature between the surface and water at 150 m were 0.13°C and 0.17°C, respectively. In April and November, the difference was less than 0.5°C.
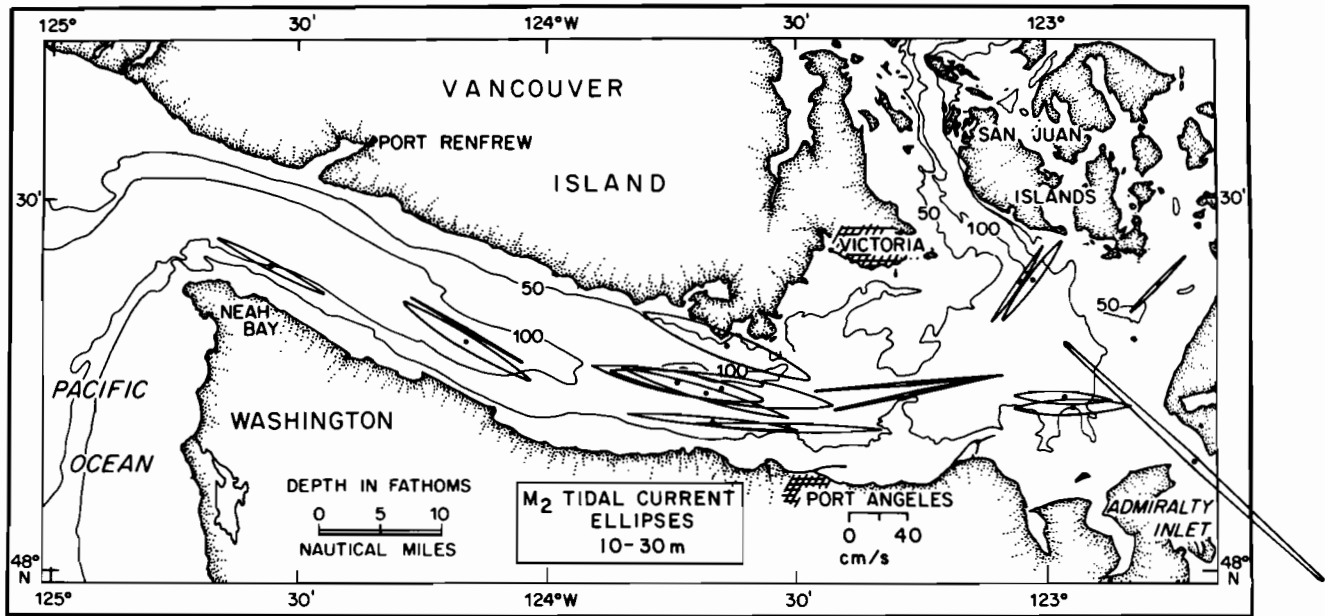
20

Figure 20.--$M_2$ tidal current ellipses at 10- to 30-m depth.

## 2.4 Tidal Currents

Tidal currents in the Strait of Juan de Fuca constitute both a navigational hazard and a primary mechanism for dispersal of spilled pollutants. A summary of existing information on tidal heights and currents in the Strait, along with a brief analysis of tidal wave behavior, has been presented by Parker (1977). In his analysis, he used the results of an intensive current and sea level monitoring program carried out from 1973-75 by the National Ocean Survey of NOAA and included previously available data. Crean (1978) numerically treated the problem of barotropic tidal behavior in the Strait, and his results give considerable insight into this complex system.

Our current observations substantiate the results of earlier analyses. Tides in the Strait of Juan de Fuca behave as a progressive wave that propagates eastward from the open ocean and whose interactions lead to semidiurnal mixed tidal currents in the eastern Strait. We present tidal currents in the form of ellipses for the entire Strait to illustrate west-east continuity (figs. 20-23). Only the major semidiurnal and diurnal components, $M_2$ and $K_1$, are shown because they contain the most energy and behave similarly to the other components. A tabulation of the five major components, $M_2$, $K_1$, $S_2$, $N_2$, and $O_1$, is presented for comparison (table 5). The constituents were computed using the first 29 days of each record listed, so they represent only the first portion of the series. Analysis of selected records in the eastern Strait has revealed that the tidal characteristics vary slightly with time over the duration of the mooring, and the values given may therefore be considered representative.

The ellipses provide a summary of tidal characteristics. We also present graphs depicting major axis amplitudes and phases for the major constituents as a function of distance landward from the mouth of the Strait (fig. 24). The $M_2$ currents were generally about 10 to 20 cm/s stronger than the $K_1$ currents throughout the entire Strait. The difference was greatest at the constriction just south of Victoria, where $M_2$ current speeds were about 60 cm/s and $K_1$ speeds were about 40 cm/s. Speeds for four major constituents were about the same at the inner and outer ends of the Strait. The highest speeds observed occurred in Admiralty Inlet (not shown) where the $M_2$ component had an amplitude of about 120 cm/s. High speeds at that location are caused by the constricted channel, which must feed a large tidal prism to the Puget Sound system to the south, and actual instantaneous current speeds at that location have been observed as high as ~300 cm/s. Throughout the region, the elongate nature of the tidal ellipses reflects the constraining influence of the lateral boundaries; in several instances the cross-channel components represented by the minor ellipse axes were of the same order as noise in

21
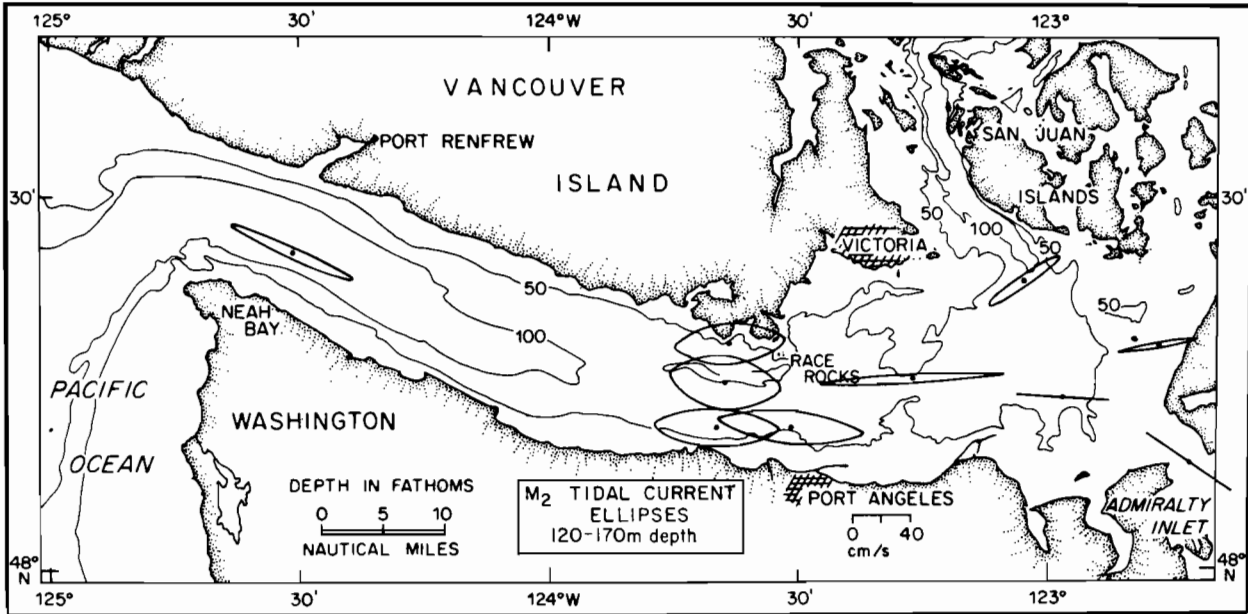
Figure 21.--$M_2$ tidal current ellipses at 120- to 170-m depth.

the current records. The only instance of appreciable rotary motion was in the near-bottom $M_2$ constituent south of Victoria. The increase in phase of the $M_2$ and $K_1$ constituents with distance up-strait demonstrates the progressive nature of the tidal wave (fig. 24). Tidal constituent amplitude increased with distance up-strait to approximately Race Rocks and decreased further eastward.

Our observed tidal currents compare favorably with those that Crean (1978) obtained with his numerical model (fig. 25). His streamlines aid in interpreting the ellipses presented
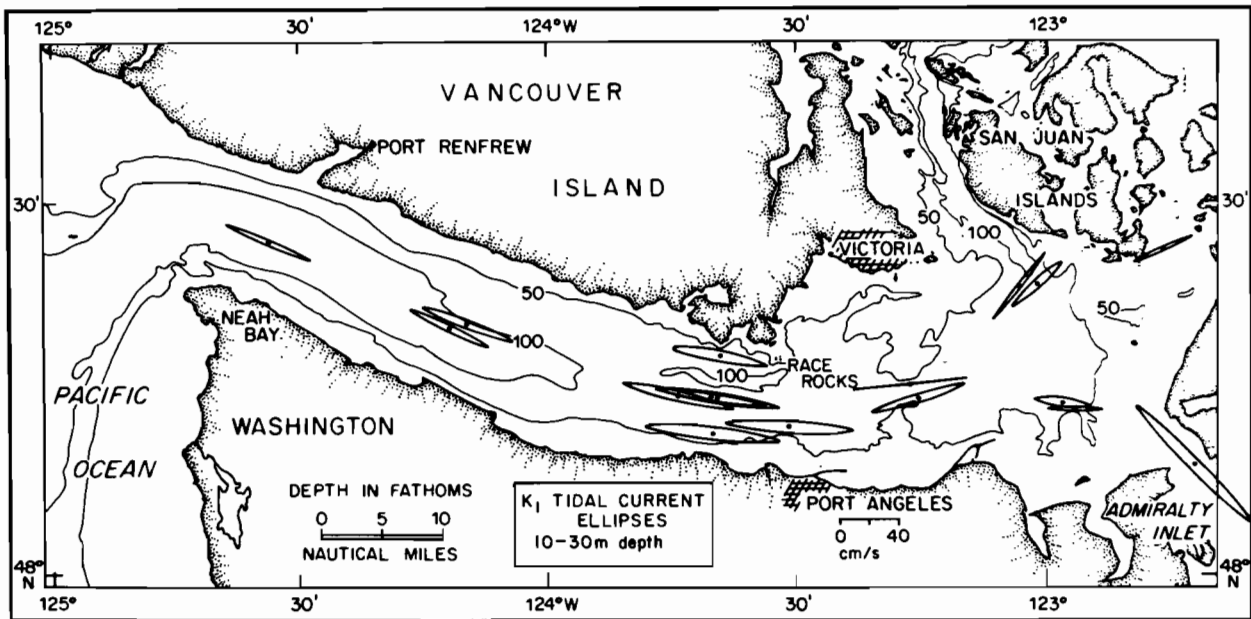


Figure 22.--$K_1$ tidal current ellipses at 10- to 30-m depth.

22
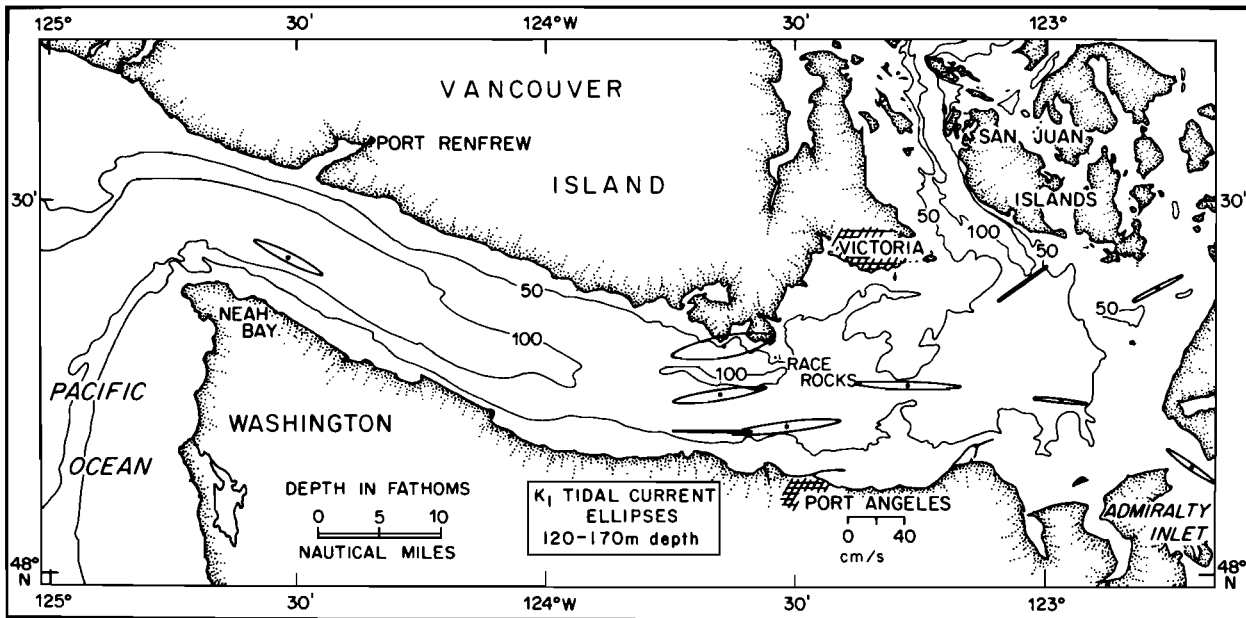
Figure 23.--$K_1$ tidal current ellipses at 120- to 170-m depth.

earlier by providing better spatial resolution. For example, the on-offshore orientation of the $M_2$ and $K_1$ ellipses just south of the San Juan Islands at Strait-9 (shown in figs. 20-23) occurs just before the streamlines curve sharply and enter Haro Strait. Of particular interest is the formation of eddies south of Victoria, at the entrance to Haro Strait, and east of New Dungeness Spit.

Ebbesmeyer et al. (1979) have summarized the historical oceanographic data in Port Angeles Harbor. Results from this study and hydraulic tidal model runs demonstrate the importance of forcing by exterior flows and local wind. Their combined effects yielded a residence time of several days to a week for near-surface water in the harbor. Net near-shore flow between New Dungeness Spit and Ediz Hook was shown to be consistently eastward or up-strait.

## 2.5 Subtidal Fluctuating Flow

Estuarine circulation is composed of both tidal and nontidal currents. Gravitational convection, an aspect of the nontidal portion, has been a topic of extensive research during past decades, since it drives the two-layer mean flow normally associated with an estuary (Officer, 1976). Between the quasi-steady-state gravitational convection and the tidal oscillations exists a broad range of time scales over which energetic motions may also occur. For this report, subtidal flow is considered to encompass current fluctuations with periods of 2 to 100 days.

Studies in other estuaries have shown that winds, atmospheric pressure, and river runoff can cause these intermediate scales of estuarine motion. For example, in Narragansett Bay, longitudinal currents with periods of 2 to 3 days were highly coherent with longitudinal winds, with currents lagging the winds by 3 h (Weisberg and Sturges, 1976). In contrast, forcing of subtidal currents in Chesapeake Bay was relatively complex (Elliott, 1978; Wang and Elliott, 1978; Wang, 1979). For time scales longer than 10 days, a significant proportion of the fluctuations was generated at the Bay mouth by along-shore coastal winds. At time scales of 4 to 10 days, both coastal and local lateral winds were important; at time scales shorter than 4 days, a longitudinal seiche motion was thought to occur. Elliott et al. (1978) found that flow near the head of Chesapeake Bay was determined by the size of the Susquehanna River discharge.

Table 5.--$M_2$, $S_2$, $N_2$, $K_1$, $O_1$ constituents for current records

| Station no. | Latitude (N) | Longitude (W) | Approx. water depth (m) | Current meter depth (m) | Series length (days) | Beginning of series | Samples per h | Type current meter | $M_2$ Major dir. (°) | Speed (cm/s) Major | Minor | Greenwich phase | Rot. | $S_2$ Major dir. (°) |
|---|---|---|---|---|---|---|---|---|---|---|---|---|---|---|
| JDF 1A S | 48°11.4' | 123°39.8' | 126.2 | 12 | 42 | 2-25-76 | 6 | A | -84.1 | 59.05 | 2.60 | 126.6 | C | -89.5 |
| JDF 2A M | 48°14.6' | 123°39.1' | 166.4 | 15 | 41 | 2-26-76 | 6 | A | -80.9 | 67.69 | 9.04 | 131.8 | C | -80.7 |
| JDF 3A N | 48°18.0' | 123°38.5' | 184.0 | 15 | 41 | 2-26-76 | 6 | A | -68.0 | 63.53 | 9.34 | 122.5 | C | -61.9 |
| JDF 13 | 48°19.5' | 124°12.0' | 205.6 | 40 | 47 | 10-29-76 | 3 | A | -60.7 | 44.66 | 0.31 | 114.5 | C | -59.5 |
| JDF 1A S | 48°11.4' | 123°39.8' | 126.2 | 121 | 42 | 2-25-76 | 6 | A | -86.7 | 44.26 | 13.66 | 93.5 | CC | -68.4 |
| JDF 2A M | 48°14.6' | 123°39.1' | 166.4 | 161 | 41 | 2-26-76 | 6 | A | -80.0 | 38.95 | 18.82 | 105.0 | CC | -55.3 |
| JDF 3A N | 48°18.0' | 122°38.5' | 184.0 | 179 | 41 | 2-26-76 | 6 | A | -94.9 | 40.20 | 14.58 | 105.8 | CC | -95.8 |
| JDF 11 | 48°26.0' | 124°30.9' | 235.9 | 170 | 44 | 12-14-76 | 3 | A | 113.8 | 45.51 | 3.57 | 59.2 | C | 111.7 |
| ST-1 | 48°14.4' | 123°40.8' | 170.0 | 10 | 81 | 2-13-76 | 8 | V | -73.5 | 58.94 | 4.04 | 124.6 | C | -62.4 |
| ST-2 | 48°15.0' | 123°44.4' | 170.0 | 10 | 101 | 11-06-76 | 8 | V | -78.8 | 59.93 | 7.25 | 115.7 | C | -79.1 |
| ST-3 | 48°26.4' | 124°33.0' | 250.0 | 10 | 101 | 11-06-76 | 8 | V | -62.5 | 41.89 | 2.74 | 105.8 | CC | -46.1 |
| ST-4 | 48°19.8' | 124°09.6' | 190.0 | 4 | 101 | 11-06-76 | 8 | V | -58.7 | 51.89 | 4.54 | 107.0 | C | -71.3 |
| MESA W | 48°25.9' | 124°31.2' | 237.7 | 76 | 45 | 6-18-77 | 3 | A | -71.9 | 45.93 | 2.06 | 137.7 | C | -74.2 |
| MESA S | 48°18.4' | 124°14.1' | 191.0 | 159 | 45 | 6-20-77 | 3 | A | -65.7 | 40.71 | 2.51 | 109.5 | CC | -75.2 |
| MESA E | 48°14.8' | 123°44.0' | 169.0 | 157 | 44 | 6-21-77 | 3 | A | -78.5 | 39.36 | 16.36 | 100.0 | CC | -50.3 |
| MESA W | 48°25.9' | 124°31.2' | 237.7 | 11 | 45 | 6-19-77 | 3 | A | -55.4 | 45.11 | 0.68 | 104.1 | C | -45.9 |
| MESA S | 48°18.4' | 124°14.1' | 191.0 | 13 | 45 | 6-20-77 | 6 | Plessey | -60.9 | 44.16 | 2.93 | 115.2 | C | -48.1 |
| MESA N | 48°22.4' | 124°09.4' | 165.0 | 30 | 45 | 6-20-77 | 3 | A | -64.2 | 17.60 | 0.63 | 102.9 | C | -70.5 |
| MESA E | 48°14.8' | 123°44.0' | 169.0 | 12 | 42 | 6-21-77 | 3 | A | -77.8 | 9.54 | 0.16 | 42.8 | CC | 114.7 |
| ST-5 | 48°15.0' | 123°46.6' | 170.0 | 10 | 97 | 6-21-77 | 8 | V | -72.7 | 62.75 | 16.54 | 114.6 | C | -70.4 |
| ST-6 | 48°26.4' | 124°33.6' | 250.0 | 10 | 73 | 6-21-77 | 8 | V | -53.5 | 42.30 | 1.04 | 96.1 | C | -41.2 |
| ST-7 | 48°20.4' | 124°13.2' | 210.0 | 10 | 97 | 6-21-77 | 8 | V | -58.2 | 29.15 | 0.91 | 100.8 | C | -49.6 |
| JDF 40 | 48°23.2' | 123°03.2' | 144.0 | 131 | 122 | 12-18-77 | 3 | A | -123.5 | 30.32 | 3.84 | 122.5 | CC | 42.5 |
| JDF 41 | 48°23.0' | 122°46.6' | 80.5 | 59 | 122 | 12-18-77 | 3 | A | -100.1 | 28.47 | 1.18 | 115.3 | CC | -3.7 |
| JDF 42 | 48°13.8' | 122°58.3' | 133.0 | 120 | 122 | 12-18-77 | 3 | A | -86.8 | 32.53 | 0.31 | 107.7 | CC | -74.1 |
| JDF 43 | 48°08.7' | 122°42.4' | 79.0 | 68 | 63 | 12-17-77 | 3 | A | -56.1 | 36.63 | 0.60 | 117.8 | CC | -53.9 |
| JDF 48 | 48°11.6' | 123°31.1' | 146.3 | 136 | 123 | 12-17-77 | 3 | A | -84.1 | 51.19 | 11.87 | 118.3 | CC | -97.5 |
| JDF 49 | 48°15.0' | 123°16.5' | 125.0 | 62 | 122 | 12-17-77 | 3 | A | -93.0 | 63.35 | 2.57 | 127.1 | C | -94.7 |
| JDF 40 | 48°23.2' | 123°03.2' | 144.0 | 31 | 122 | 12-18-77 | 3 | A | 34.7 | 33.99 | 1.31 | -42.5 | CC | 38.5 |
| JDF 41 | 48°23.0' | 122°46.6' | 80.5 | 29 | 122 | 12-18-77 | 3 | A | -135.9 | 27.63 | 2.09 | 129.4 | CC | 25.6 |
| JDF 42 | 48°13.8' | 122°58.3' | 133.0 | 30 | 122 | 12-18-77 | 3 | A | -87.9 | 33.75 | 3.82 | 129.6 | C | -81.3 |
| JDF 43 | 48°08.7' | 122°42.4' | 79.0 | 28 | 101 | 12-17-77 | 3 | A | -47.5 | 121.97 | 3.50 | 119.2 | C | -43.6 |
| JDF 48 | 48°11.6' | 123°31.1' | 146.3 | 23 | 123 | 12-17-77 | 3 | A | -88.3 | 64.75 | 2.52 | 125.0 | C | -97.4 |
| JDF 49 | 48°15.0' | 123°16.5' | 125.0 | 32 | 122 | 12-17-77 | 3 | A | -95.0 | 65.64 | 1.70 | 127.8 | C | -94.0 |
| ST-8 | 48°14.4' | 123°15.6' | 130.0 | 10 | 119 | 12-19-77 | 8 | V | -102.0 | 57.41 | 1.17 | 116.9 | CC | -101.2 |
| ST-9 | 48°23.4' | 123°01.8' | 150.0 | 10 | 23 | 12-19-77 | 8 | V | 37.4 | 34.32 | 3.77 | -51.2 | C | 42.8 |
| ST-10 | 48°13.2' | 122°57.0' | 120.0 | 10 | 119 | 12-19-77 | 8 | V | -91.1 | 40.48 | 5.54 | 116.5 | C | -97.3 |
| JDF 51 | 48°22.9' | 122°46.8' | 84.0 | 30 | 85 | 7-11-78 | 6 | A | 52.3 | 37.55 | 1.61 | -30.3 | CC | 50.4 |
| JDF 52 | 48°14.6' | 122°58.9' | 133.5 | 30 | 84 | 7-13-78 | 6 | A | -85.7 | 40.74 | 3.64 | 124.0 | C | -75.4 |
| JDF 53 | 48°08.7' | 122°42.3' | 77.0 | 45 | 82 | 7-11-78 | 6 | A | -47.4 | 71.44 | 1.16 | 135.4 | C | -50.7 |
| ST-11 | 48°13.2' | 123°05.4' | 130.0 | 10 | 41 | 7-16-78 | 8 | V | -74.8 | 46.30 | 1.28 | 110.2 | C | -86.0 |
| ST-12 | 48°20.4' | 122°58.2' | 110.0 | 10 | 39 | 7-16-78 | 8 | V | -114.2 | 45.08 | 19.27 | 117.1 | C | -110.1 |
| ST-13 | 48°14.4' | 122°57.6' | 140.0 | 10 | 106 | 7-16-78 | 8 | V | -83.3 | 41.74 | 8.65 | 113.5 | C | -74.0 |
| JDF 51 | 48°22.9' | 122°46.8' | 84.0 | 60 | 69 | 7-12-78 | 6 | A | -85.1 | 30.70 | 2.03 | 93.3 | C | 50.1 |
| JDF 52 | 48°14.6' | 122°58.9' | 133.5 | 60 | 84 | 7-13-78 | 6 | A | -84.4 | 36.12 | 2.59 | 126.5 | CC | -88.2 |
| JDF 53 | 48°08.7' | 122°42.3' | 77.0 | 60 | 72 | 7-11-78 | 6 | A | -52.2 | 55.73 | 3.29 | 132.1 | C | -52.5 |

24

Table 5.--$M_2$, $S_2$, $N_2$, $K_1$, $O_1$ constituents for current records (continued)

| $S_2$ (cont.) | | | | | $N_2$ | | | | | $K_1$ | | | | | $O_1$ | | | |
| Speed (cm/s) | | Greenwich phase | Rot. | Major dir. (°) | Speed (cm/s) | | Greenwich phase | Rot. | Major dir. (°) | Speed (cm/s) | | Greenwich phase | Rot. | Major dir. (°) | Speed (cm/s) | | Greenwich phase | Rot. |
| Major | Minor | | | | Major | Minor | | | | Major | Minor | | | | Major | Minor | | |
|---|---|---|---|---|---|---|---|---|---|---|---|---|---|---|---|---|---|---|
| 13.75 | 2.91 | 143.6 | C | -103.0 | 15.62 | 4.25 | 116.6 | CC | -83.7 | 46.73 | 4.08 | 17.5 | CC | 88.2 | 18.64 | 0.76 | 177.2 | CC |
| 17.05 | 1.79 | 155.5 | C | -76.8 | 20.11 | 0.73 | 104.6 | C | -80.8 | 43.80 | 3.55 | 30.0 | C | -81.7 | 23.39 | 0.42 | 16.9 | CC |
| 18.70 | 0.51 | 132.2 | CC | -32.8 | 13.86 | 0.39 | 103.7 | CC | -78.9 | 32.70 | 3.76 | 50.0 | C | -73.2 | 26.52 | 2.38 | 30.0 | CC |
| 11.39 | 0.82 | 149.2 | C | -45.2 | 4.24 | 0.22 | 78.8 | CC | -64.5 | 30.00 | 1.19 | 13.3 | C | -64.0 | 17.18 | 1.37 | -4.3 | C |
| 11.35 | 4.94 | 114.3 | CC | -45.4 | 6.59 | 1.32 | 61.7 | C | -89.4 | 27.28 | 0.31 | 16.1 | CC | 45.2 | 12.75 | 0.79 | 154.6 | C |
| 8.88 | 6.98 | 108.9 | CC | -73.2 | 7.42 | 3.69 | 58.1 | CC | -99.4 | 33.03 | 3.17 | 22.2 | CC | 84.8 | 18.80 | 1.57 | 160.3 | CC |
| 9.56 | 3.79 | 138.3 | CC | -84.5 | 6.55 | 1.52 | 65.9 | CC | 78.3 | 36.57 | 7.24 | 187.2 | CC | 85.6 | 20.50 | 3.32 | 145.8 | CC |
| 14.36 | 1.71 | 88.0 | C | -65.0 | 13.76 | 0.89 | -19.3 | C | -63.1 | 26.42 | 2.62 | 112.5 | C | -61.8 | 17.68 | 1.68 | 7.5 | C |
| 15.55 | 1.58 | 129.9 | CC | -54.1 | 16.14 | 1.53 | 73.1 | CC | -82.4 | 38.60 | 2.41 | 25.7 | C | -86.6 | 23.05 | 5.53 | 20.1 | C |
| 12.27 | 1.91 | 151.9 | C | -58.7 | 14.99 | 0.95 | 81.8 | C | -75.9 | 38.71 | 3.41 | 17.1 | C | -75.5 | 18.43 | 2.36 | 4.8 | CC |
| 8.57 | 1.95 | 136.2 | C | -107.2 | 5.26 | 4.31 | 116.7 | CC | -66.2 | 31.86 | 0.18 | 11.6 | C | -65.1 | 16.96 | 0.00 | -10.2 | CC |
| 9.63 | 1.09 | 136.4 | C | -43.8 | 10.63 | 0.10 | 82.8 | CC | -68.7 | 33.59 | 2.71 | 8.6 | C | -59.0 | 20.02 | 5.85 | -9.1 | C |
| 11.86 | 1.89 | 149.1 | C | -79.1 | 9.86 | 0.15 | 126.5 | C | -64.4 | 28.68 | 1.74 | 14.6 | C | -65.7 | 16.76 | 2.79 | 25.8 | C |
| 10.28 | 0.01 | 137.4 | CC | -64.0 | 7.44 | 0.10 | 73.7 | CC | -68.1 | 24.76 | 0.18 | 12.5 | CC | -63.7 | 12.69 | 0.31 | -7.1 | CC |
| 8.78 | 4.41 | 95.8 | CC | -93.9 | 7.01 | 3.93 | 81.1 | CC | -87.3 | 27.28 | 2.61 | 12.4 | CC | 100.2 | 15.34 | 3.81 | 162.0 | CC |
| 12.80 | 2.92 | 124.6 | C | -44.3 | 9.27 | 0.51 | 70.6 | C | -66.9 | 26.63 | 1.34 | 15.0 | CC | -57.3 | 11.76 | 3.98 | -4.1 | CC |
| 8.97 | 0.27 | 137.8 | CC | -61.3 | 8.77 | 1.68 | 73.0 | C | -65.7 | 26.95 | 0.30 | 18.8 | C | -60.6 | 17.79 | 1.78 | -10.2 | C |
| 4.93 | 1.36 | -18.8 | C | -63.2 | 14.80 | 0.68 | 137.7 | C | -70.4 | 10.68 | 0.09 | 10.5 | C | -59.2 | 4.80 | 0.19 | 21.7 | CC |
| 28.94 | 6.95 | 41.8 | C | -74.8 | 6.12 | 2.96 | 95.7 | C | 111.5 | 6.29 | 1.38 | 108.0 | CC | 98.1 | 8.01 | 2.91 | 43.4 | CC |
| 16.72 | 6.60 | 139.8 | C | -69.5 | 12.23 | 5.33 | 89.7 | C | -64.9 | 34.86 | 6.87 | 18.0 | C | -83.3 | 20.32 | 1.55 | 24.8 | C |
| 10.76 | 1.45 | 127.2 | C | -51.6 | 8.40 | 0.66 | 60.5 | C | -65.0 | 24.10 | 1.86 | 5.7 | CC | -60.9 | 11.72 | 3.05 | -25.0 | CC |
| 2.14 | 1.31 | 189.9 | CC | -56.0 | 9.98 | 0.08 | 100.3 | C | -64.0 | 17.18 | 0.22 | 8.9 | CC | -49.0 | 10.40 | 2.15 | 16.8 | C |
| 9.76 | 2.62 | -14.0 | CC | -164.2 | 5.18 | 0.45 | 82.6 | C | 54.7 | 20.91 | 0.68 | 191.6 | CC | 26.8 | 12.90 | 6.28 | 147.9 | C |
| 4.96 | 1.34 | 29.2 | CC | -107.6 | 6.72 | 1.18 | 98.7 | C | 62.7 | 18.90 | 1.34 | 194.5 | CC | 54.0 | 12.53 | 2.00 | 156.1 | C |
| 10.76 | 2.51 | 128.4 | C | -94.2 | 7.90 | 1.94 | 79.1 | CC | -84.4 | 18.40 | 0.98 | 1.6 | C | 93.7 | 12.58 | 0.80 | 155.8 | CC |
| 42.06 | 1.28 | 143.9 | C | 122.5 | 35.64 | 2.47 | 133.2 | C | -54.1 | 20.73 | 1.28 | -24.6 | C | -46.4 | 14.13 | 1.90 | 2.9 | C |
| 12.03 | 1.84 | 146.3 | CC | -85.2 | 11.02 | 0.02 | 82.8 | C | -97.0 | 37.60 | 2.67 | 13.5 | CC | 82.8 | 22.32 | 2.64 | 174.3 | C |
| 16.48 | 0.25 | 155.6 | CC | -96.9 | 12.84 | 0.76 | 91.5 | C | -88.9 | 36.94 | 2.27 | 18.1 | C | -83.7 | 16.69 | 0.55 | -0.3 | C |
| 7.03 | 1.55 | -21.1 | CC | -140.8 | 7.48 | 2.48 | 113.8 | CC | 37.9 | 25.14 | 1.60 | 213.9 | CC | 23.8 | 11.59 | 2.30 | 207.6 | CC |
| 7.17 | 2.49 | -20.8 | C | -130.0 | 6.11 | 1.22 | 105.2 | CC | 66.4 | 22.04 | 1.38 | 189.4 | CC | 93.0 | 12.27 | 5.55 | 139.9 | CC |
| 6.65 | 1.15 | 163.6 | C | -93.4 | 5.43 | 0.44 | 89.2 | C | -82.3 | 19.16 | 3.73 | 34.9 | C | -87.1 | 12.06 | 1.23 | 28.9 | CC |
| 44.26 | 3.56 | 113.0 | C | -45.3 | 20.07 | 1.65 | 137.8 | CC | -44.9 | 57.05 | 4.07 | 10.0 | CC | -35.2 | 35.71 | 8.50 | -3.0 | CC |
| 17.63 | 0.68 | 162.0 | CC | -92.5 | 13.63 | 0.08 | 91.8 | CC | -87.1 | 43.97 | 2.90 | 29.6 | C | -85.2 | 27.29 | 1.05 | 4.7 | C |
| 16.85 | 0.04 | 152.1 | CC | -101.3 | 15.10 | 1.01 | 94.7 | C | -96.0 | 39.46 | 0.04 | 25.7 | CC | -95.3 | 19.55 | 1.38 | 7.4 | CC |
| 16.96 | 1.15 | 146.4 | C | -119.9 | 12.78 | 0.32 | 86.4 | CC | -107.2 | 33.05 | 2.52 | 19.3 | CC | 71.7 | 15.79 | 4.91 | 173.3 | CC |
| 9.80 | 0.63 | 190.6 | CC | 26.7 | 7.61 | 0.69 | -61.9 | CC | 48.7 | 22.50 | 3.24 | 204.6 | CC | 49.8 | 11.87 | 0.11 | 183.8 | CC |
| 7.95 | 1.50 | 152.1 | C | -81.3 | 6.95 | 1.40 | 107.3 | C | -89.1 | 18.97 | 1.32 | 24.9 | C | -74.2 | 13.96 | 3.07 | 17.1 | C |
| 8.77 | 1.28 | -0.4 | C | -113.9 | 5.95 | 0.80 | 120.0 | C | 66.3 | 26.06 | 3.60 | 188.7 | CC | 84.7 | 15.02 | 5.32 | 177.5 | CC |
| 10.61 | 2.06 | 144.3 | C | -83.0 | 7.37 | 0.57 | 99.3 | C | -85.9 | 19.39 | 2.47 | 24.8 | C | -89.1 | 9.87 | 1.46 | 19.7 | C |
| 20.27 | 1.44 | 137.8 | C | -48.8 | 13.09 | 0.16 | 114.3 | CC | -46.9 | 29.50 | 0.56 | 9.3 | CC | -42.6 | 15.15 | 1.70 | 20.7 | C |
| 13.02 | 2.30 | 146.8 | CC | -76.8 | 10.30 | 1.57 | 78.3 | CC | -93.6 | 28.84 | 2.34 | 25.1 | C | -85.2 | 17.63 | 0.64 | 4.7 | CC |
| 11.30 | 3.30 | 151.0 | C | -108.8 | 11.15 | 4.57 | 89.4 | C | -91.1 | 15.68 | 4.93 | 27.6 | C | 61.5 | 13.26 | 2.64 | 180.8 | C |
| 16.26 | 2.12 | 157.2 | C | -80.3 | 8.99 | 0.84 | 84.3 | C | -80.1 | 25.54 | 7.95 | 31.6 | C | -82.8 | 14.69 | 0.56 | 0.2 | CC |
| 8.13 | 1.65 | -35.2 | C | -97.5 | 4.59 | 0.73 | 57.4 | CC | 70.4 | 16.16 | 4.29 | 178.4 | CC | 55.1 | 11.65 | 2.40 | 138.0 | C |
| 7.80 | 0.56 | 137.9 | CC | -83.0 | 7.37 | 0.57 | 99.3 | C | -85.9 | 19.39 | 2.47 | 24.8 | C | -89.1 | 9.87 | 1.46 | 19.7 | C |
| 16.73 | 0.28 | 139.4 | CC | -47.5 | 9.17 | 0.44 | 113.9 | C | -45.9 | 25.71 | 0.58 | 16.4 | C | -44.3 | 11.29 | 0.52 | 28.1 | CC |
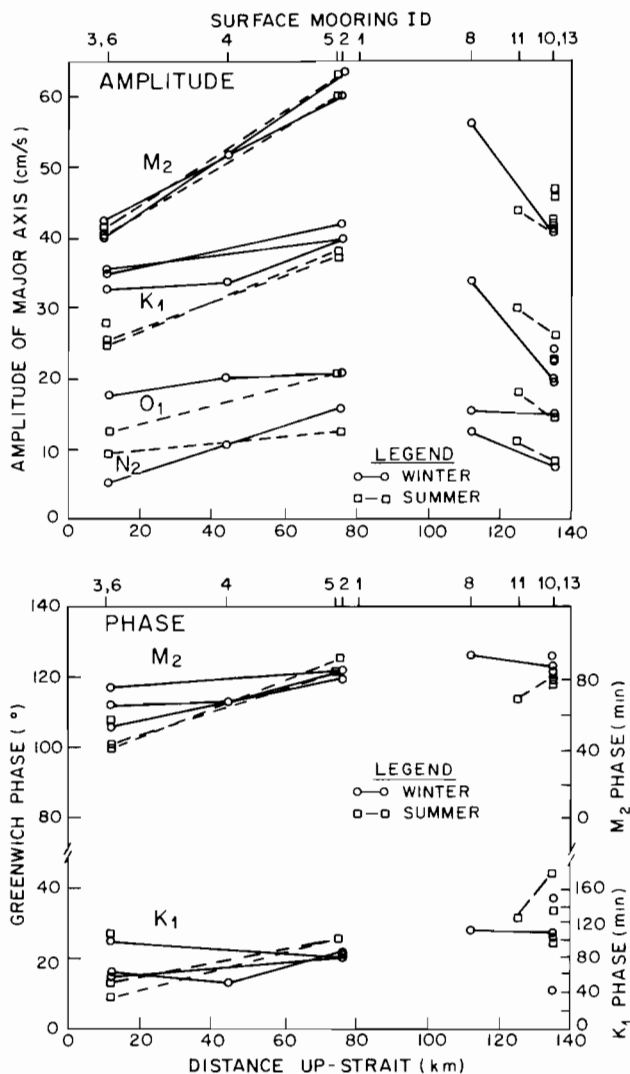
Figure 24.--$K_1$ tidal current amplitudes ($M_2$, $K_1$, $O_1$, $N_2$) and phases ($M_2$, $K_1$) for the major constituents (as computed from selected current records) as a function of distance landward from the mouth of the Strait.

Results in this section demonstrate the importance of coastal wind forcing and the relative lack of influence by local winds and river runoff in the Strait of Juan de Fuca. One of Cannon's (1978) principal findings was that large-amplitude, long-period current flucuations occurred in the western Strait particularly in winter. These motions caused the net seaward estuarine flow in the surface layer to reverse for periods up to 10 days, causing eastward intrusions of coastal ocean water as far as 90 km from the mouth and retention of surface water within the system. These events were related to coastal storms and followed periods of strong southwesterly winds off the Washington coast (Holbrook and Halpern, 1977; Holbrook et al., 1980). They penetrated the eastern basin to an undetermined extent.

### 2.5.1 Subtidal current observations

In the eastern Strait, the spatial distribution of subtidal current variance did not vary appreciably with season in contrast to the vast difference in subtidal variance between winter and summer measured in the western Strait (Holbrook et al., 1980). The vertical and horizontal distribution of subtidal current fluctuations can best be seen by examining currents measured at locations A and G (see fig. 2). Examples of subtidal along-strait current fluctuations during winter and summer at sites A and G are contrasted in fig. 26. Throughout this section, tidal and higher frequency fluctuations have been removed by applying a $A_{25}^2 A_{24}$ Godin low-pass filter (Godin, 1973), which has a half-amplitude frequency of 0.0143 cph. The largest current fluctuations occurred at 4-m depth at site A near the mouth
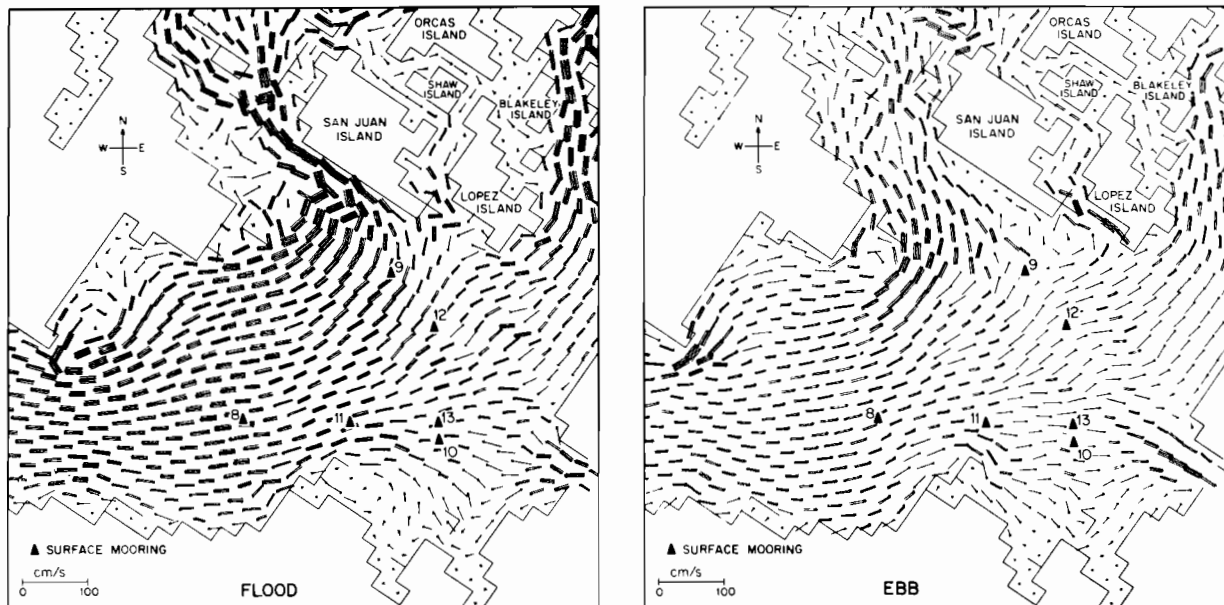
26

*Figure 25.—Typical flood and ebb currents computed from barotropic tidal model, showing locations of surface current moorings.*

of the Strait during winter, where subtidal current reversals accounted for 35% of the filtered record, lasted from 3 to 10 days, and had maximum up-strait speeds of 25 to 55 cm/s. During winter 1977-78 at site G, three periods of up-strait flow were measured that lasted from 2 to 7 days and had maximum up-strait speeds of 5 to 30 cm/s. Between June and August at site A, the along-strait components of near surface and lower layer currents exhibited less variability than during fall, winter, and spring. No reversals occurred at sites A or G during these months. During September at site A, quasi-steady-state summer conditions ended, and three reversals occurred. The longer period fluctuations were generally 180° out of phase between the surface and deep layers. The amplitude of the deep layer currents was much smaller than that of the near-surface currents.

The longitudinal distribution of subtidal current variance in the near-surface and deep layer is shown in fig. 27. Subtidal variance decreased with depth in the near-surface layer, especially in the western Strait during winter when the variance was primarily confined to the upper 40 m of the water column. During summer in the western Strait and throughout the year in the eastern Strait, subtidal variance below 50-m depth was less than 50 $cm^2/s^2$. Thus, the estimated subtidal rms amplitude about the mean estuarine flow in the deep layer was less than 7 cm/s throughout the system. Fluctuations in the surface layer were larger and were related to meteorological events (see discussion of wind forcing in this section).

Horizontal coherence between mooring sites in the eastern Strait was weak. For example, coherence squared estimates over the most energetic region of the spectrum (centered at 0.00323 cph) between 4-m currents at ST-8 and ST-9 and at ST-8 and ST-10 were 0.57 and 0.55, respectively. Over the entire subtidal frequency range approximately 19% and 18%, respectively, of the variance was coherent between these pairs, with all the coherent variance occurring in the east-west component; no estimate for the north-south components was significant at the 95% level. In contrast, over the tidal frequencies, 85% and 95% of the variance were coherent.

Vertical coherence was much higher than horizontal coherence at all mooring sites, with 85% to 95% of the subtidal variance significantly coherent in the upper layer. For example, coherence estimates over the most energetic region of the spectrum (centered at 0.00323 cph) between 4 and 20 m at ST-9 and ST-10 were 0.93 and 0.94, respectively.

In summary, the distribution of subtidal variance in the eastern Strait may be characterized as less intense than in the western Strait, with weak horizontal and strong vertical
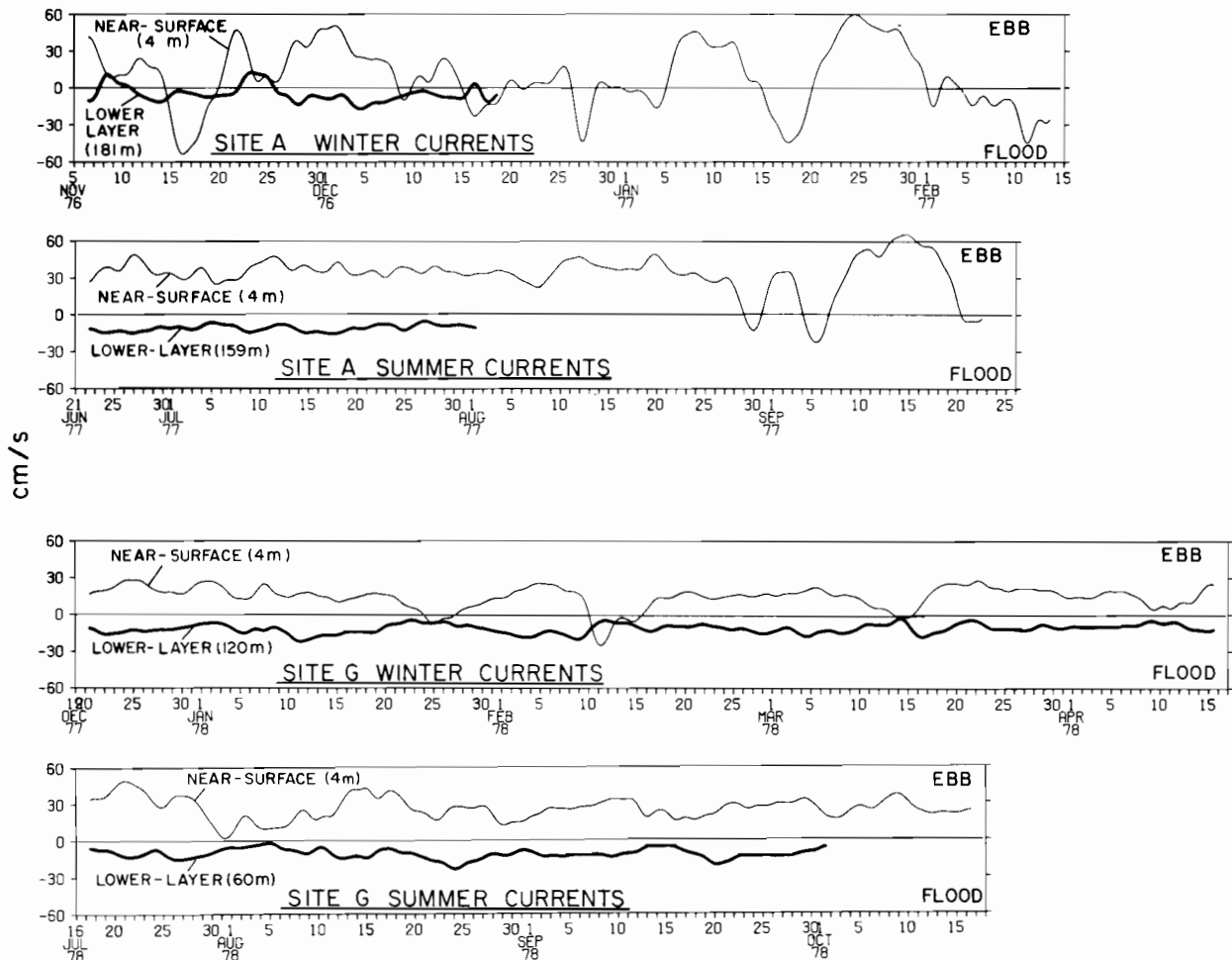
27

*Figure 26.--Along-strait subtidal currents at sites A and G during winter and summer. Tidal and higher frequency fluctuations have been removed by applying an $A_{25}^2 A_{24}$ Godin (1973) low-pass filter. Up-strait flow is negative.*

coherence in the near-surface layer. The low level of horizontal coherence is not necessarily surprising, since bottom and lateral topographic features are extremely irregular. Also, the appropriate horizontal scale for internal motions as defined by the internal Rossby radius of deformation was estimated to be between 2 and 10 km, which was less than the horizontal spacing of the moorings.

## 2.5.2 Wind observations

Over-the-water and coastal wind measurements were made during winter 1977-78 and summer 1978 in conjunction with current observations in the eastern basin of the Strait. Over-the-water winds were measured and recorded by vector-averaging wind recorders 4 m above the water from surface buoys located at sites 8 through 13 (fig. 6). Winds were measured and recorded onshore by Aanderaa wind recorders at Smith Island, New Dungeness Spit, and Tatoosh Island. Winds measured at permanent weather stations operated by the U.S. National Weather Service and Environment Canada were used to supplement the time series data. The coastal wind field was estimated from a 3° by 3° atmospheric pressure grid centered at 48°N, 125°W, 25 km off the Washington coast (Bakun, 1978, personal communication). Surface frictional effects were approximated by rotating the wind vectors 15° counterclockwise and reducing speeds by 30%.
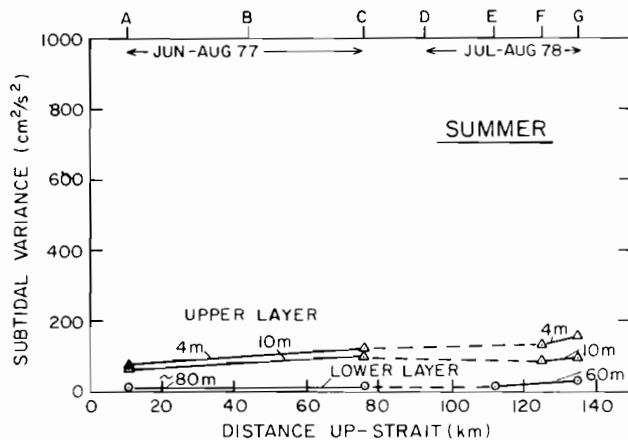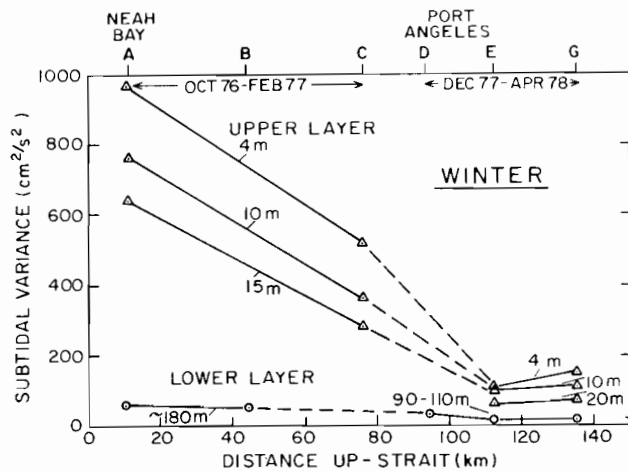
28

Figure 27.--Longitudinal distribution of subtidal variance during winter and summer. Subtidal variance was primarily confined to the upper 40 m of the water column.

During the winter experiment, winds along the Washington coast were predominantly south-easterly, reflecting offshore cyclonic activity. The maximum computed wind was 24.7 m/s toward 333° TN on 9 February 1978. Winds measured at the buoy sites and shore stations in the Strait were easterly, with the exception of brief periods of strong westerlies associated with frontal passages. The strongest winds were recorded on 5 January, with maximum shore wind speeds of 21.9, 19.1, and 14.4 m/s at Race Rocks, New Dungeness, and Smith Island, respectively. Coincident maximum over-the-water winds were 19.8, 17.9, and 17.3 m/s at ST-8, 9, and 10, respectively. During this storm, a winter 1977-78 maximum atmospheric pressure difference of 8 mb was observed between Bellingham and Quillayute airports. In the eastern Strait, westerly winds generally decreased in strength with distance eastward as a result of orographic effects. In the regions east of the buoy sites, southerly winds from Puget Sound influenced the local wind field.

During the summer experiment, coastal winds were northwesterly, reflecting the offshore Pacific high. Winds in the Strait were westerly and had an additional superposed 5 to 10 m/s afternoon sea breeze on most days. The amplitude of the sea breeze was least in the eastern Strait. By late August storm activity had increased, and between 23 and 26 August a low pressure system centered 500 km off the Washington coast generated southerly winds of more than 13 m/s for several days. This storm occurred during a 4-day study period when surface currents were intensively monitored (see section 2.5).

Statistical comparisons between winds measured at the buoy sites and at the National Weather Service remote shore locations revealed that winds throughout the region were similar at any given time. Over-the-water winds were significantly correlated with coastal winds at the 95% level, with east-west components having higher correlation coefficients (R = 0.6 to 0.8) than north-south components (R = 0.4 to 0.6). Over-the-water wind speeds were weaker,

29

typically 60% to 80% of the coastal wind speeds. Uncorrelated fluctuating wind components had root-mean-square amplitudes of 2 to 3 m/s. The correlations between over-the-water winds and different nearby coastal winds were similar. For example, correlation coefficients between the east-west components of winds measured at ST-8 and New Dungeness and Port Angeles were 0.62 and 0.56, respectively.

### 2.5.3 Local wind forcing

The near-surface current response to the local wind field was weak but statistically significant at the 95% level. The squared coherence between the over-the-water winds and the near-surface currents (at 4-, 10-, 20-m depth) at ST-8 was 0.46 at periods longer than 8 days for east-west winds and currents and between 0.52 and 0.72 at periods of 1.4 to 2.9 days for east-west winds and north-south currents. In all, 18% of the subtidal current fluctuations at ST-8 at 4-m depth were related to the local winds. Poorer coherences were computed for ST-9 and ST-10 during winter. Although the current response nearer the surface was undoubtedly more dramatic, measurements in this study showed a weak relationship between the local winds and near-surface currents. The strongest local winds of the winter occurred on 5 January, when westerly wind speeds exceeded 15 m/s for several hours. These winds caused the vertical mean shear between 4 and 10 m at ST-8 and ST-10 to decrease from 1 cm/s/m to approximately zero. However, the net flow remained westward at all measured depths in the near-surface layer. Similar fluctuations in the vertical shear were recorded during other strong westerlies. This response decreased with depth, and the vertical shear change between 10- and 20-m depths was smaller. This lack of local wind forcing may be due in part to the limited duration (usually a few hours) of strong winds in the Strait.

### 2.5.4 Nonlocal meteorological forcing

A principal result of experiments conducted in the western Strait was the finding that the near-surface and deeper subtidal current fluctuations were highly coherent with coastal winds (Cannon, 1978; Holbrook and Halpern, 1977; Holbrook et al., 1980). This relationship can be reviewed by examining time series of coastal winds and along-strait currents in the western Strait during winter, as shown in fig. 28. Vertical lines are drawn at times of maximum near-surface up-strait current reversal at site A. Maximum near-surface current reversals at site C lagged those at site A by 47 h, indicating an up-strait propagation velocity of 37 cm/s. Periods of deceleration in the along-strait flow before maximum reversal are coincident with south-southwesterly coastal winds and rising sea level near the Strait entrance at Neah Bay and Port Renfrew. These data suggest that an Ekman flux mechanism was responsible for the generation of these reversals, which then slowly propagated up-strait. Maximum up-strait reversals were accompanied by a reversal in the vertical current shear making them near-surface baroclinic phenomena. No phasing was observed in the deeper layer, which also responded to coastal winds, suggesting that the barotropic response in the near-surface layer was masked by the larger amplitude baroclinic response.

An important characteristic of coastal forcing is the directionality of the offshore winds, which generates the response. Figure 29 shows squared coherence spectra between computed coastal winds and along-strait currents at sites A and C. Contours of squared coherence are drawn as a function of wind direction (positive axis represents direction toward which wind blows). Maximum squared coherence was found over the most energetic portion of the spectrum (periods of 12 days) when the winds were along a 020° to 200° TN axis. The squared coherence estimates (95% confidence interval) were 0.90 (0.70 to 0.96) at site A and 0.73 (0.34 to 0.88) at site C. The current response lagged (±95% confidence interval) the coastal winds by 39 (±6) h at site A and by 91 (±23) h at site C. Totals of 71% and 44% of the along-strait subtidal variability at sites A and C, respectively, were attributed to coastal winds along an 020° to 200° TN axis. Table 6 summarizes other statistics between the records shown in fig. 28. It is noteworthy that coastal winds from the southeast (toward 350° to 300° TN) did not generate a strong current response in the Strait over the long-period time scales.

Although the impact of coastal forcing on circulation was less dramatic in the eastern Strait than in the western Strait, it still represented a principal driving force of subtidal current reversals. As in the western Strait, the frequency and strength of up-strait flow reversals in the eastern Strait decreased with distance eastward. Representative time series of near-surface currents in the eastern Strait at sites D (JDF48) and G (ST-10) as well as
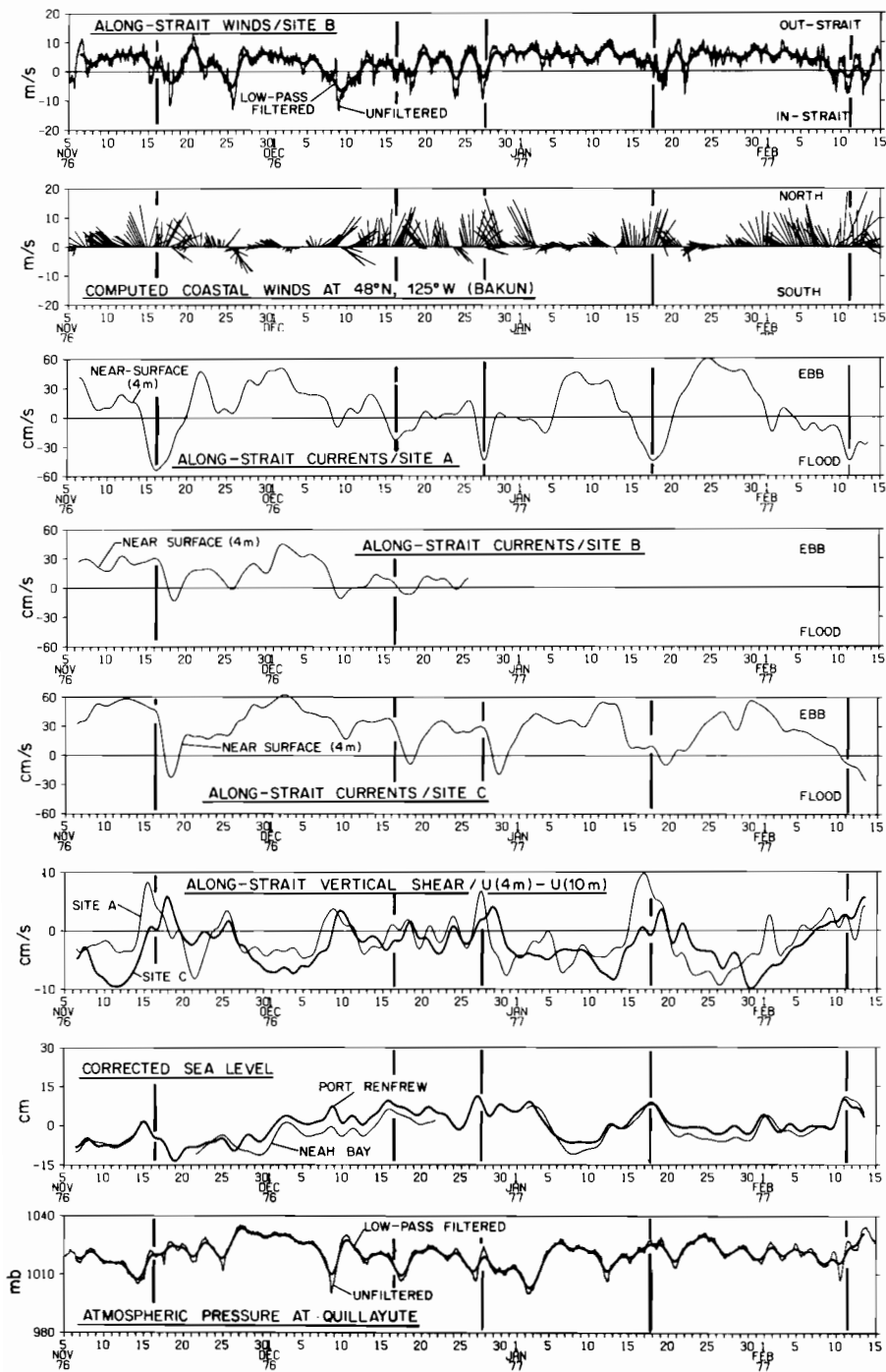
Figure 28.--Low-pass filtered time series of local winds, near-
surface and deep currents, vertical current shear between 4
and 10 m, computed geostrophic coastal winds, corrected sea
level at Port Renfrew and Neah Bay, and atmospheric pressure
at various sites.  Vertical lines indicate times of maximum
up-strait (negative) current flow at site A.  Periods of
deceleration in the along-strait direction, before maximum
current reversal, are coincident with SSW coastal winds and
rising corrected sea level at Port Renfrew and Neah Bay.

31
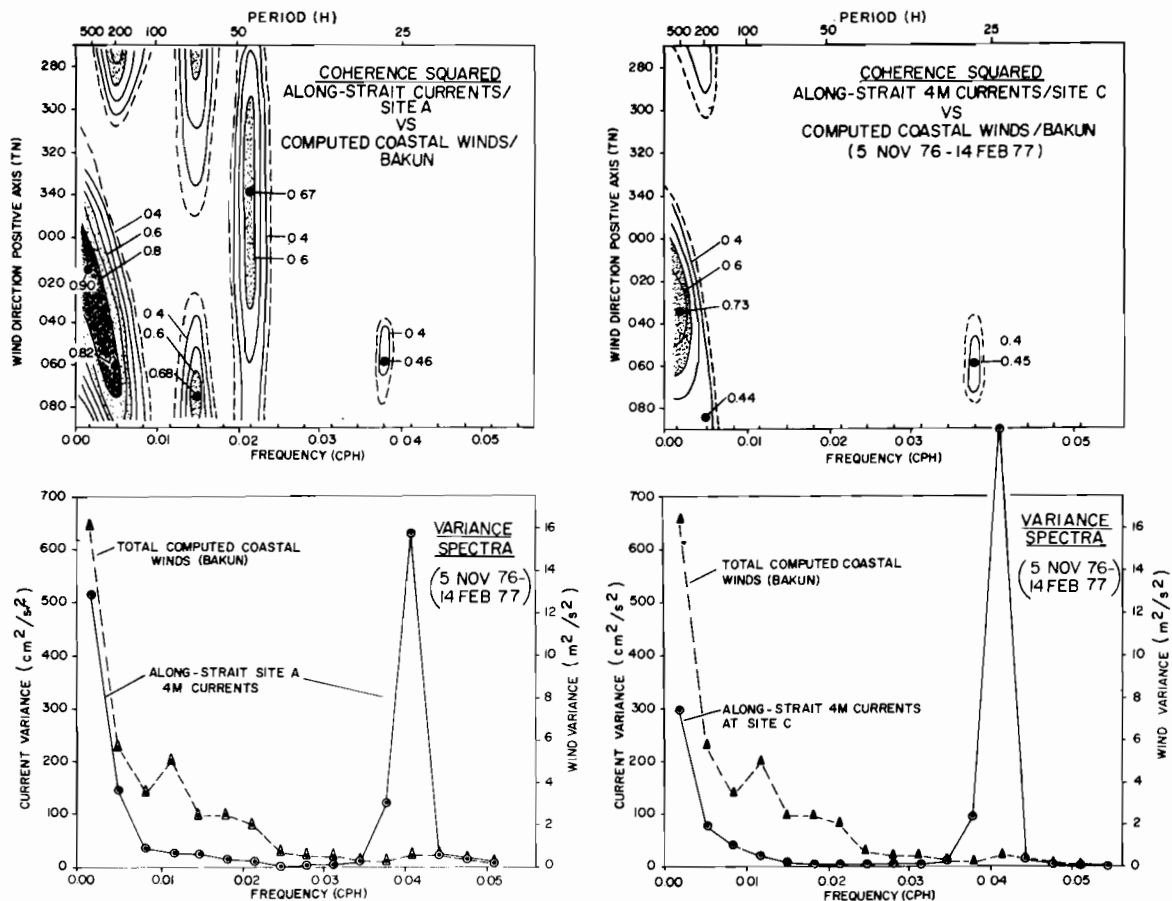
*Figure 29.--Squared coherence spectra (above) for 6-h values of computed geostrophic coastal winds (Bakun, 1977) and 6-h average along-strait currents and density spectra (below) at sites A and C. Maximum subtidal coherence occurred with coastal winds directed along a 020°-200° axis.*

local and computed coastal winds are shown in fig. 30. Vertical lines are drawn at times of maximum up-strait reversal at site D. Seven periods of reversed currents at 23-m depth at site D accounted for 16% of the subtidal record, lasted from 2 to 4 days, and had maximum speeds of 6 to 18 cm/s. At 4-m depth at site G, 44 km up-strait, three reversals accounted for 14% of the subtidal record, lasted from 4 to 6 days, and had maximum speeds of 6 to 27 cm/s.

Although all seven reversals at site D occurred after periods of southerly coastal winds, the direction and duration of these winds played an important role in both reversal strength and up-strait penetration distance. As seen in fig. 29, the response to southeasterly coastal winds was weak whereas south-southwesterly winds generated the largest coherencies. During winter 1977-78, coastal winds were predominantly southeasterly with only brief periods of southwesterly flow. Consequently, reversals in the eastern Strait were not as large as might be expected during other winters. Three reversals at site G followed periods of south-southwesterly winds. Although some of the strongest southeasterly winds occurred on 7-8 January, the induced reversal was not measured at site G, despite the additive effects of a strong up-strait wind stress. One of the clearest examples of coastal forcing occurred in March, when southerly coastal winds of more than 15 m/s blew for several days (6-8 March) and were preceded and followed by periods of relative calm. The maximum reversal was meas-ured at site D on 10 March, nearly 4 days after commencement of southerly coastal winds. The relative effects of wind strength are seen during periods of southerly winds that vary in strength on 15-17 and 23-27 March.

Although coastal low pressure systems with southwesterly winds occur more frequently and persist longer during winter than during summer, occasionally a low pressure system will sit

32

*Table 6.--Squared coherence and phase between local and coastal winds, currents, vertical current shear, corrected sea level, and atmospheric pressure shown in fig. 28*

| | Along-strait currents (cm/s) | | | | | Current shear (cm/s) | | Corrected sea level (cm) | Atmospheric pressure (mb) | |
|---|---|---|---|---|---|---|---|---|---|---|
| | | | | | | A (4-10 m) | C (4-10 m) | Port Renfrew | QA | BA-QA |
| | A/4 m | A/181 m | B/4 m | B/178 m | C/4 m | | | | | |
| Record length (days) | 102 | 41 | 51 | 42 | 102 | 102 | 102 | 102 | 102 | 102 |
| **Computed coastal wind along 020°-200° at 48°N, 125°W (Bakun)** | | | | | | | | | | |
| Variance[1] | 553 | 41 | 5 | 41 | 207 | 8.0 | 5.3 | 5.1 | 3.0 | 0.48 |
| % total[2] | 71 | 70 | 2 | 78 | 44 | 40 | 36 | 15 | 7 | 27 |
| Phase lag[3] (h) | 39 | 0 | 1 | -3 | 91 | 29 | 88 | -12 | 0[6] | 12 |
| 95% conf. | 6 | 20 | 4 | 9 | 23 | 30 | 29 | 13 | 2 | 3 |
| **Along-strait local wind at site B** | | | | | | | | | | |
| Variance[1] | 121 | 11 | 124 | 11 | 52 | 9.2 | 7.7 | 1.8 | 1.7 | 1.7 |
| % total[2] | 16 | 21 | 56 | 22 | 11 | 46 | 52 | 6 | 4 | 94 |
| Phase lag[3] (h) | -3 | 8[4] | -34 | -5[4] | -28 | 21 | -33 | 3[5] | 13 | -9 |
| 95% conf. | 10 | 3 | 13 | 5 | 15 | 39 | 27 | 2 | 2 | 5 |

[1] Subtidal variance (cm²/s², cm², mb²) coherent at 95% level.
[2] Percent of total subtidal variance coherent at 95% level.
[3] Phase lag (with 95% confidence interval) of estimate containing most coherent variance. Positive phase means winds lead coherent series.
[4] Up-strait winds lead maximum out-strait currents in lower layer by indicated phase lag.
[5] Up-strait winds lead high water at Port Renfrew by 3 h.
[6] Northward coastal winds occur at the same time as low pressure at Quillayute.

off the coast long enough during summer to generate a response in the Strait. Such a system was observed during 20-27 August 1978 (fig. 31). South-southwesterly winds associated with this system generated a near-surface, up-strait current reversal that was observed 4 to 6 days later in the eastern Strait. In fig. 32 a vertical line is drawn at the time of arrival of the maximum reversal at site D to illustrate the phase lag of this response relative to the coastal winds and currents farther up-strait. The reversal was measured at site F 39 h later than at site D, giving an up-strait phase velocity of 21 cm/s in the eastern Strait. The currents at site G did not reverse (Holbrook et al., 1980).

Before and during up-strait propagation of the storm-induced reversal, an intensive 4-day study period was carried out, during which surface currents were monitored using the Coastal Ocean Dynamics Analysis Radar (CODAR) and surface drifters. In this study NOAA, Environment Canada, and MESA-contracted scientists investigated in greater detail the near-surface circulation in the Strait to provide an intercomparison of direct and remote sensing techniques for measuring near-shore currents, and to provide observational data for testing the Puget Sound surface circulation model.

The CODAR system, which consisted of two shore-based, transportable HF Doppler radars, remotely mapped hourly surface currents over a 900-km² area with a spatial resolution of 1.2 km (Barrick et al., 1977). Measurements were made between Point Wilson and New Dungeness for 3 days and between New Dungeness and Port Angeles for 1 day. Although analysis of this data set is continuing, preliminary comparisons between the near-surface currents measured by VACM's at the three surface mooring sites and the CODAR data show good agreement for both the mean and tidal flows. The 3-day average (23-25 August) flow (fig. 33) showed net seaward velocities of 20 to 40 cm/s throughout the eastern Strait. Examples of typical flood and ebb surface currents as measured by the CODAR system are shown in fig. 34; because of the additive effects of estuarine circulation, the ebbs are stronger and floods weaker than those computed from Crean's model (fig. 25). This pattern was consistent with most of the near-surface current data during this period. The sub-
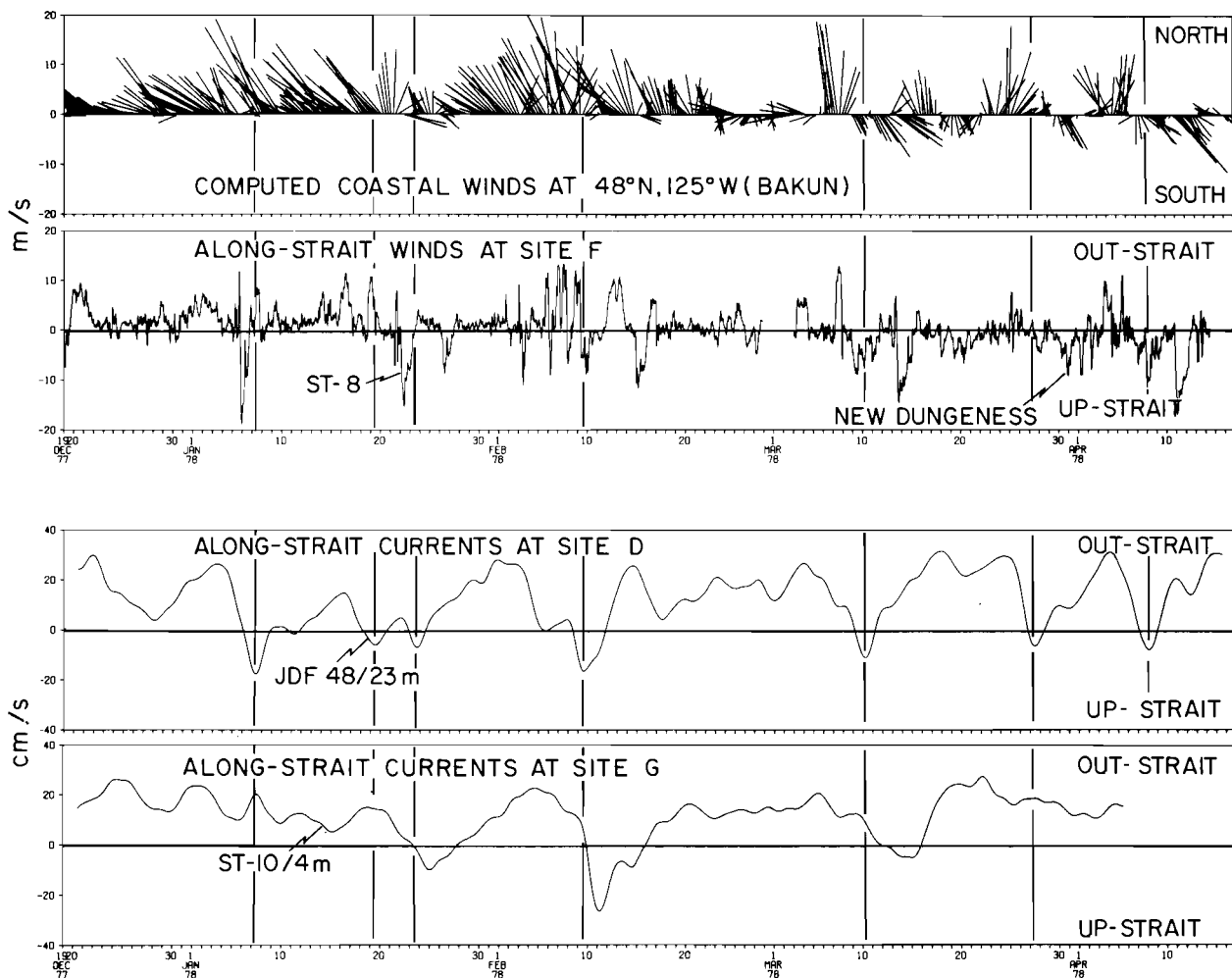
*Figure 30.--Low-pass filtered time series of near-surface currents at sites D and G, and unfiltered local and coastal winds during winter. Vertical lines are drawn at times of maximum up-strait reversal at site D. Extent to which coastal winds affected flow in eastern basin depended on their strength, duration, and direction.*

sequent 24-h average CODAR current map in fig. 35 corresponded to the time of arrival of the reversal between Port Angeles and New Dungeness 3 days later. The core of the eastward flow was located near mid-strait, with shoreward components on either side. In the convergence zone near the reversal front, the seaward estuarine flow was diverted southward with an eastward recirculation north of New Dungeness Spit. This CODAR map dramatically illustrates the complexity of current reversals and suggests their potential effect on the movement of foreign material transported by surface currents.

Surface drifter trajectories tracked by Canadian investigators (Ages, personal communication, 1979) also showed a net seaward drift before the storm's effects and a landward (eastward) drift as the reversal propagated through the western Strait (fig. 36). Up-strait excursions of more than 35 km over a 24-h period were observed. Other surface drifter studies (Cox et al., 1978) showed an intensification of the flood tidal flow north of the New Dungeness Spit on 26 August, which was associated with the reversal.

In summary, the field observations demonstrated the role of nonlocal meteorological forcing in modifying circulation in an estuary opening onto the Pacific continental shelf. Winds conducive to coastal downwelling (southwesterlies) generated a current response in the Strait that was larger than the net gravitational circulation and led to current reversals that
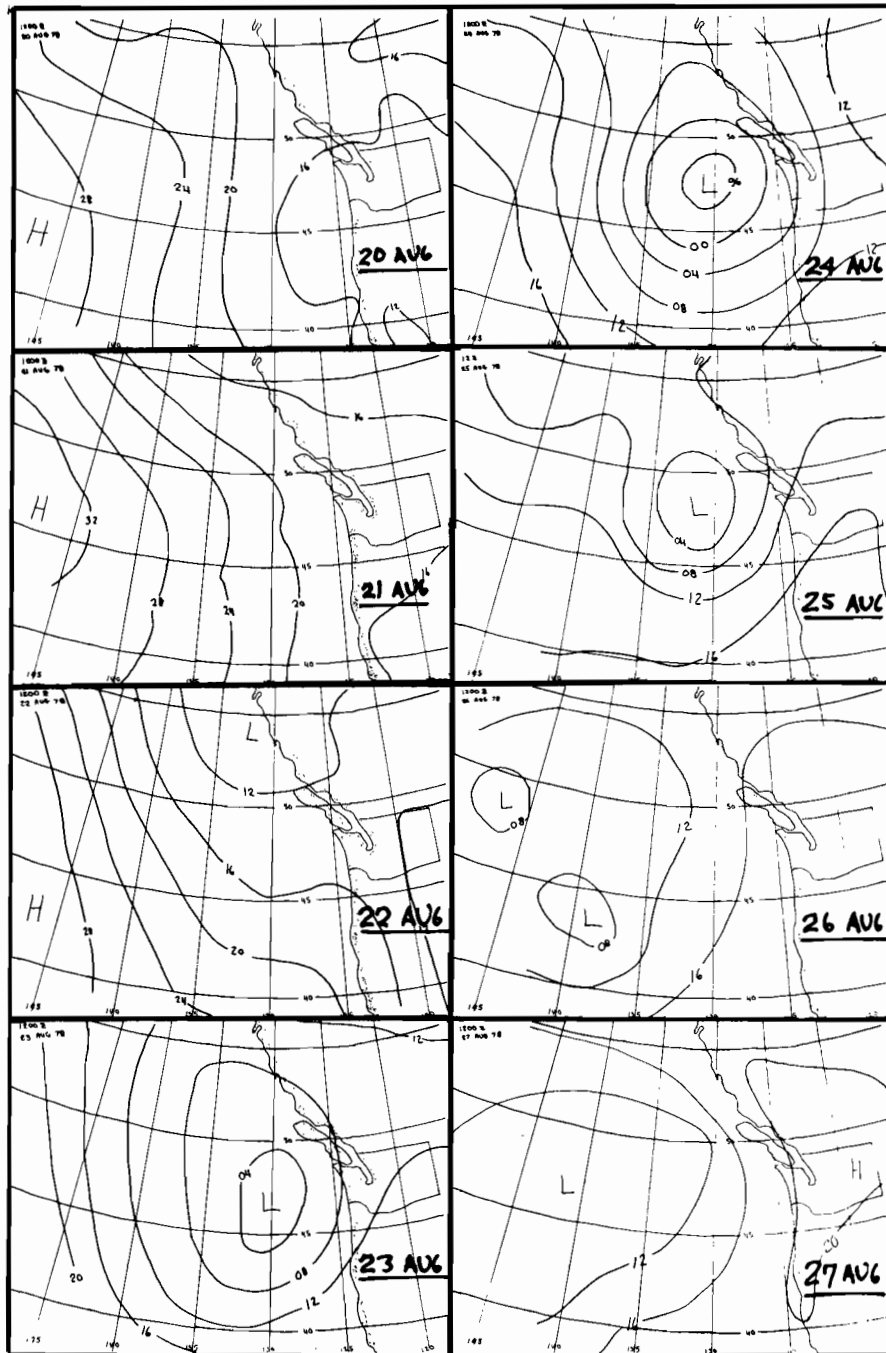
34

*Figure 31.--Surface pressure maps showing stationary low pressure system centered 300-400 km off the Washington coast between 23 and 25 August 1978.*

propagated up-strait. Although the current variance associated with coastal wind forcing decreased with distance up-strait and with depth, the effects of coastal storms were observed as far as 135 km up-strait. Since southerly coastal winds occurred with lower frequency and intensity during summer, subtidal current reversals were rare between June and August. In contrast, local along-strait winds were weakly coherent with subtidal current fluctuations and can be considered secondary to coastal forcing in modifying the near-surface circulation. It should be noted that the moored current measurements were not made at depths shallower than 4 m, and therefore the effects of local winds on surface currents may be greater.
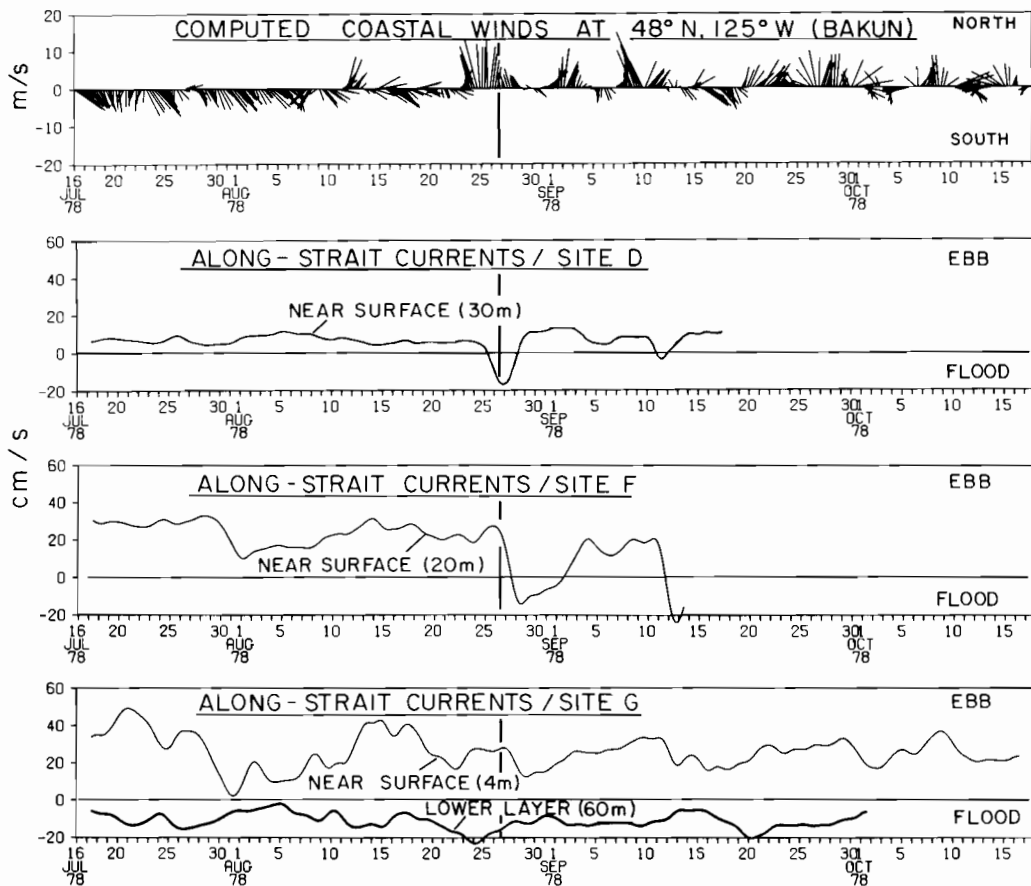
Figure 32.--SSW coastal winds associated with the offshore low-pressure
system (fig. 31) generated an along-strait current reversal at sites D
and F. A vertical line is drawn at the time of arrival of the reversal
at site D and illustrates the phase lag of this response relative to
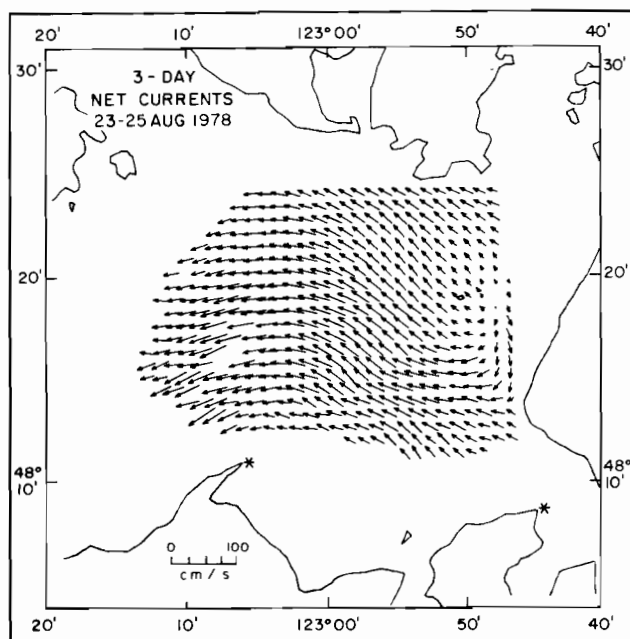coastal winds and currents farther up-strait.



Figure 33.--Three-day averaged surface
currents as measured by CODAR. Aster-
isks mark locations of the two shore-
based HF Doppler radar units. The
pattern of new seaward velocities of
20-40 cm/s was consistent with near-
surface current measurements.

36
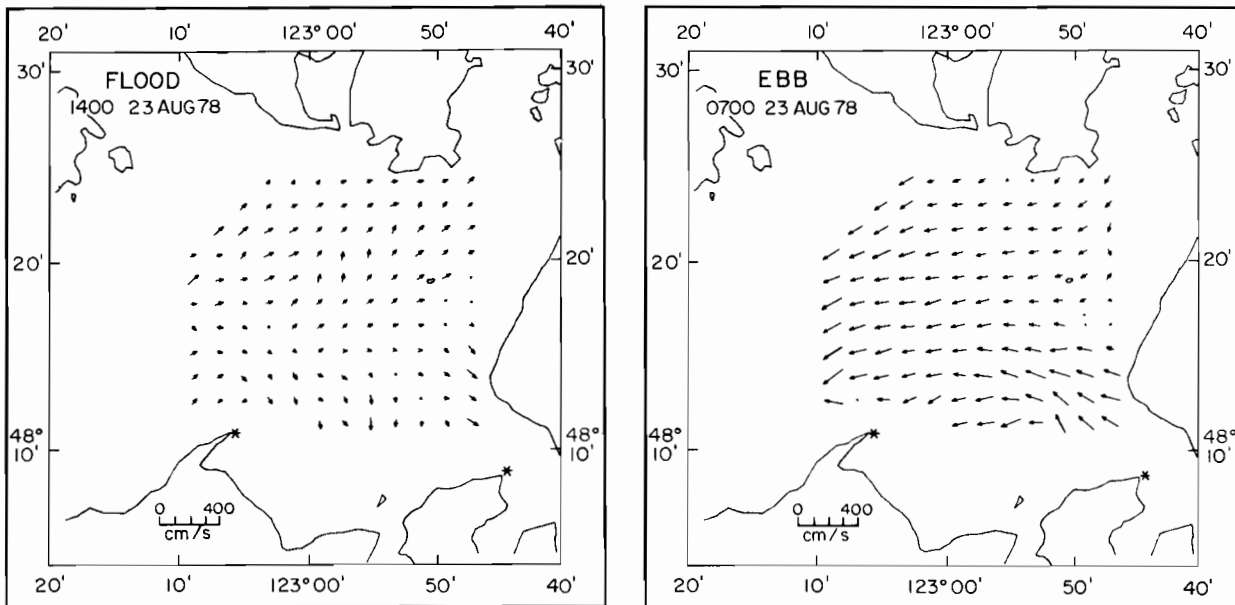
Figure 34.--Typical flood and ebb surface current maps as measured by the CODAR.

## 2.6 Freshwater Effects on Currents

Although freshwater runoff from the Fraser River (which was assumed to represent the regional river discharge) varied widely with season (fig. 6), the induced net circulation varied little between summer and winter. As an example, the vertical distributions of mean currents at site G (shown in fig. 12) were nearly identical in winter and summer. Nearer the coast at site A, the upper layer outflow reflected the additional effects of coastal forcing discussed earlier in this section. This lack of direct response to variation in river runoff can be addressed by applying steady-state gravitational circulation theory (Hansen and Rattray, 1965; Officer, 1976). Holbrook and Halpern (1980) have used this theory to show that the
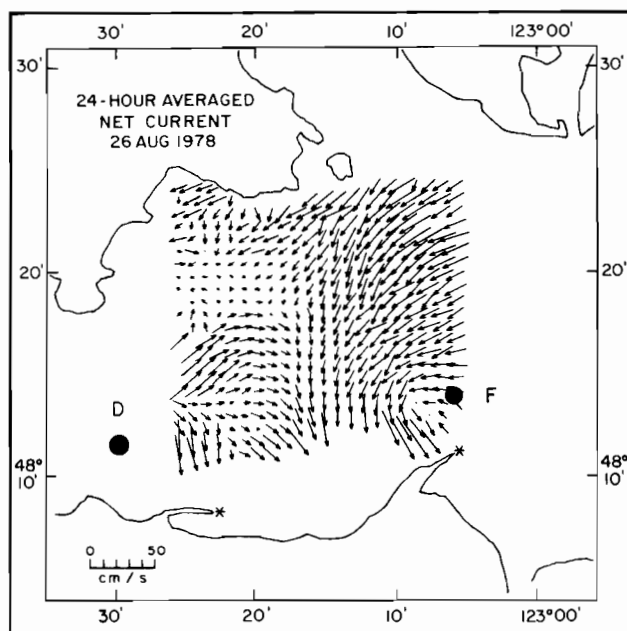


Figure 35.--Twenty-four hour averaged surface currents on 26 August measured by CODAR. This period corresponds to time of arrival of current reversal shown in fig. 32 in this area. The core of the reversal (eastward flow) was located near mid-strait with shoreward components on either side. In the convergence zone near the reversal front, the seaward estuarine flow was diverted southward with an eastward recirculation north of New Dungeness Spit.
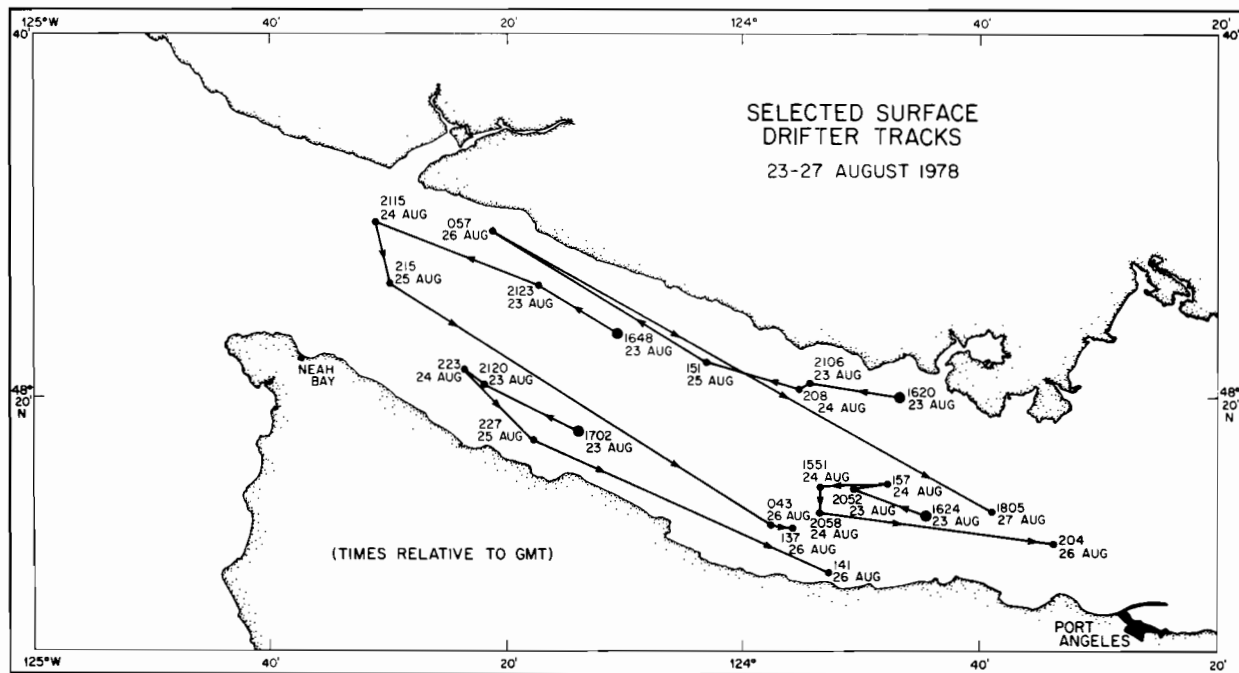
37

*Figure 36.--Surface drifter trajectories tracked by Canadian investigators during the period following the coastal storm shown in fig. 31.*

direct effects of river runoff on the sea surface slope are insignificant ($\sim 10^{-2}$ smaller) when compared with the indirect effects of runoff on the salinity distribution and therefore, the longitudinal density gradients. Thus, only the indirect effects of fresh water on the internal mass field are important. Efforts to measure seasonal changes in the longitudinal density field using CTD survey data and to relate them to subtidal current fluctuations were not successful, due in part to tidal aliasing and the limited number of cruises. In general, gradients were larger during summer than winter; however, the statistical confidence limits were too large to allow meaningful conclusions.

## 3. CONTINUING STUDIES

A major result of the study described by Cannon (1978) and this report (section 2.5) was the discovery of large amplitude (25 to 55 cm/s), low-frequency current fluctuations that over-shadowed the net circulation in the Strait during much of the year. These low-frequency motions were manifested in the near-surface layer by prolonged reversals in the estuarine circulation, during which intrusions of coastal oceanic waters propagated eastward at 20 to 30 cm/s throughout the Strait. The intruded waters were relatively warmer and fresher during fall and winter months and contained coastal species of zooplankton and phytoplankton. These current fluctuations are well correlated to coastal atmospheric forcing off the Washington coast (see section 2.5.4). Our knowledge concerning spatial and seasonal distribution of the reversals is limited by the relatively short records (compared with the observed 10- to 100-day oscillations) that have been collected near midchannel and by the lack of any near-shore time series current measurements. Historical wave and tide height records also suggest that our moorings in the western Strait were deployed during an atypical winter when storm activity was unusually quiet, and therefore, the magnitude and extent of the reversals may be much greater during normal seasons. It is unknown whether the coastal winds directly force the along-strait, low-frequency fluctuations through an Ekman flux mechanism near the mouth or indirectly through coastal sea level fluctuations induced by either (1) Ekman dynamics on the continental shelf, i.e., downswelling; (2) partial blockage by Vancouver Island of the northward flowing Davidson Current; or (3) northward propagating free and/or forced conti-nental shelf waves. Concurrent coastal and Strait time series measurements are necessary to examine and sort out these generating mechanisms.

38

In early 1979, scientists from the Institute of Ocean Sciences (IOS) at Patricia Bay, Vancouver Island, began an extensive oceanographic study off the west coast of Vancouver Island. Three lines of current moorings are being maintained normal to the coast to continuously monitor the upper, middle, and bottom layer currents for a period of 1 to 1½ yr. This is the first major current survey conducted off the Canadian west coast. Physical oceanographic features that will be studied include the following: (1) continental shelf waves, (2) internal baroclinic tides, (3) prevailing ocean currents, (4) surface tidal currents, (5) water properties and oceanic fronts, and (6) ocean turbulence. B. Hickey, University of Washington, also investigated atmospheric forcing of continental shelf circulation along the Washington coast.

In concert with the Canadian and University of Washington studies, PMEL (with MESA support) began in March 1979 a 15-mo cooperative experiment to examine the seasonal and spatial distribution of the low-frequency, near-surface currents in the western Strait of Juan de Fuca, and to relate them to continental shelf circulation along Vancouver Island and the Washington coast and to sea level and sea level gradient fluctuations within the Strait. Portions of this study will be conducted jointly with scientists from IOS and will take advantage of the extensive set of concurrent oceanographic measurements from the continental shelf.

Analysis of the CODAR data set is continuing, in conjunction with the other physical measurements obtained in August 1978. Expected analyses include (1) a comparison between near-surface currents measured by the CODAR system, current meters, and surface drifters, (2) a spatial analysis of tidal currents, and (3) a study of the effects of local wind forcing on surface currents.

## 4. SUMMARY AND CONCLUSIONS

Cannon (1978) summarized research results accumulated during the past 15 yr for the Strait of Juan de Fuca. His discussion primarily focused on the western basin, the region where most measurements had been made up to that time. Winter and summer experiments were subsequently conducted during 1977-78 in the eastern basin. This report describes the principal water motions that were identified and observed.

It was found that over time scales of 4 to 25 h, tidal currents dominated water motions throughout the Strait of Juan de Fuca. From 58% to 99% of the current variability can be explained by tidal oscillations in the Strait. The four principal tidal components in the eastern basin were $M_2$, $K_1$, $O_1$, and $N_2$. Amplitudes varied from 40 to 60, 20 to 35, 15 to 20, and 8 to 14 cm/s, respectively (fig. 24). Canadian numerical tidal model studies have shown the complexity of these currents as they flow across the irregular bottom topography and through confined passages (fig. 25). The tidal currents can exceed 200 to 250 cm/s (4 to 5 kn) in the more restricted passages of the San Juan Islands and in Admiralty Inlet. Around near-shore and over-shoal regions, eddies and tidal fronts can become locally important; however, they have received little study, and circulation details remain undetermined.

Superposed on the tidal motions are the estuarine and wind-driven currents which, over time scales longer than 1 day, play a principal role in transporting surface trapped and suspended pollutants. The effects of these motions in modifying the tidal ebb and flood currents are apparent when outputs from Crean's barotropic tidal model and the CODAR surface current maps are compared. The estuarine circulation consisted of a well developed two-layer pattern, with near-surface velocities directed seaward at 20 to 40 cm/s and deep layer velocities directed landward at 10 cm/s. The level of no net motion varied between 40- and 60-m depth. The surface manifestation of this estuarine pattern was a broad westward transport of surface water, which supports the commonly held concept that surface trapped material should move seaward. However, the daily ebbing and flooding tidal currents greatly complicate this picture. Eddies, fronts, and complex recirculation patterns make the prediction of trajectories difficult and limited in accuracy. Results from drift card studies illustrate this, since landings are distributed on beaches peripherally throughout the entire eastern Strait.

Local winds had a minimal role in generating near-surface currents. Although the winds were coherent with and helped to maintain the vertical current shear, only a small percentage of the current fluctuations at 4-m depth were directly related to measured, over-the-water winds. The surface currents are undoubtedly affected to a greater degree, but moored current measurements in this study do not allow a simple extrapolation to the surface.

One of the most significant findings of this study was the effect of coastal storms on circulation in the eastern basin. Moored current meter observations during winter 1977-78 showed that seven current reversals leading to up-strait subtidal surface flow occurred for 2- to 6-day periods, with maximum speeds of 20 cm/s. These reversals occurred subsequent to south-southwesterly storm winds along the coast and were associated with rising sea level at the mouth of the Strait. The extent to which coastal winds affected flow in the eastern basin depended on their strength, direction, and duration. Reversals were observed as far as 135 km from the Strait entrance at site G.

Although coastal low pressure systems with southwesterly winds occurred more frequently and persisted longer during winter than summer, occasionally a low pressure system dominated the coast long enough during summer to generate a response in the Strait. Such a system was present between 23 and 25 August 1978, during an intensive study period. South-southwesterly coastal winds generated a near-surface current reversal that was observed 4 to 6 days later in the eastern Strait. The 24-h averaged CODAR current map corresponding to the time of arrival of the reversal between Port Angeles and New Dungeness dramatically showed the reversal of normal seaward flow of surface water. Complexity near the reversal front was evidenced by the diverted southward estuarine flow that appeared to recirculate eastward off New Dungeness Spit. Surface drifters showed first a net seaward drift before the storm's effects, and then a landward (eastward) drift as the reversal propagated through the western Strait and into the eastern Strait. These field observations demonstrate the major role that nonlocal meteorological forcing can play in modifying circulation in an estuary opening onto the Pacific continental shelf.

Observations presented in this report imply that a spill resulting from a tanker accident within the Strait could impact the ecologically sensitive near-shore zone and beaches before flushing into the coastal ocean. Intrusions of coastal water generated by coastal winds are common during winter and have been observed year-round; therefore, an oil slick could have an eastward trajectory well into the eastern basin region. Because of the complex pattern of eddies, fronts, and shore-directed current components, the potential for oil slick beaching increases with eastward distance into the system.

## 5. ACKNOWLEDGMENTS

## 6. REFERENCES

Barrick, D. E., M. W. Evans, and B. L. Weber (1977): Ocean surface currents mapped by radar. Science 198:4313.

Cannon, G. A., ed. (1978): Circulation in the Strait of Juan de Fuca; some recent oceanographic observations. NOAA Tech. Rep. ERL-PMEL 29, 49 pp.

Cannon, G. A., and N. P. Laird (1978): Circulation in the Strait of Juan de Fuca, 1976-1977. (Unpublished manuscript.)

Cox, J. M., C. C. Ebbesmeyer, and J. M. Helseth (1978): Surface drift sheet movements observed in the inner Strait of Juan de Fuca, August 1978. NOAA Tech. Memo. ERL-MESA 35, 104 pp.

Crean, P. B. (1978): A numerical model of barotopic mixed tides between Vancouver Island and the mainland and its relation to studies of the estuarine circulation. In Hydrodynamics of Estuaries and Fjords, J. Nihoul, ed., Elsevier, Amsterdam, 283-313.

Ebbesmeyer, C. C., J. M. Cox, J. M. Helseth, L. P. Hinchey, and D. W. Thomson (1979): Dynamics of Port Angeles Harbor and approaches, Washington. Prepublication manuscript, MESA Puget Sound Project, Seattle, Washington, 104 pp.

Elliott, A. J. (1978): Observations of the meteorologically induced circulation in the Potomac estuary. Est. Coastal Mar. Sci. 6:285-299.

Elliott, A. J., D-P. Wang, and D. W. Pritchard (1978): The circulation near the head of Chesapeake Bay. J. Mar. Res. 36:643-655.

Fissel, D. E. (1976): Pressure differences as a measure of currents in Juan de Fuca Strait. Pac. Mar. Sci. Rep. 76-17, Institute of Ocean Sciences, Patricia Bay, Victoria, B.C., 63 pp. (Unpublished manuscript.)

Fissel, D. E., and W. S. Huggett (1976): Observations of currents, bottom pressures and densities through a cross-section of Juan de Fuca Strait. Pac. Mar. Sci. Rep. 76-6, Institute of Ocean Sciences, Patricia Bay, Victoria, B.C., 68 pp. (Unpublished manuscript.)

Godin, G. (1973): The analysis of tides. University of Toronto Press, Toronto, Canada, 264 pp.

Halpern, D. (1980): Moored current measurements in the upper ocean. In Instruments and Methods in Air-Sea Interaction, R. E. Davis, F. W. Dobson, and L. Hasse, eds., Plenum, New York. (In press.)

Halpern, D., and R. D. Pillsbury (1976): Influence of surface waves upon subsurface current measurements in shallow water. Limnol. Oceanogr. 21:611-616.

Hansen, D. V., and M. Rattray, Jr. (1965): Gravitational circulation in straits and estuaries. J. Mar. Res. 23:104-122.

Harris, R. G., and M. Rattray, Jr. (1954): The surface winds over Puget Sound and the Strait of Juan de Fuca and their oceanographic effects. Univ. of Wash. Tech. Rep. 37, 101 pp.

Herlinveaux, R. H., and J. P. Tully (1961): Some oceanographic features of Juan de Fuca Strait. J. Fish. Res. Board Canada 18:1027-1071.

Holbrook, J. R., and D. Halpern (1977): Observations of near-surface currents, winds and temperature in the Strait of Juan de Fuca during November 1976-February 1977. Trans. Amer. Geophys. Union 53:1158.

Holbrook, J. R., and D. Halpern (1980): Observations of local and non-local atmospheric forcing in the western Strait of Juan de Fuca during winter. (In preparation.)

Holbrook, J. R., R. D. Muench, and G. A. Cannon (1980): Seasonal observations of low-frequency atmospheric forcing in the Strait of Juan de Fuca. In Fjord Oceanography; Proceedings of a NATO Workshop, Plenum, New York. (In press.)

Huggett, W. S., J. F. Bath, and A. Douglas (1976): Data record of current observations, Vol. XV, Juan de Fuca Strait 1973. Institute of Ocean Sciences, Patricia Bay, Victoria, B.C., 169 pp. (Unpublished manuscript.)

Krancus, G. A., C. A. Pearson, and R. L. Charnell (1978): One-pass processing system for Aanderaa current meter data. Second Working Conference on Oceanographic Data Systems, UNOLS, WHOI, Woods Hole, Mass., 96-111.

Maunder, W. J. (1968): Synoptic weather patterns in the Pacific Northwest. Northwest Sci. 42:80-88.

McCullough, J. R. (1975): Vector averaging current meter speed calibration and recording technique. WHOI Tech. Rep. 75-44. (Unpublished manuscript.)

Muench, R. D., and D. T. Heggie (1978): Deep water exchange in Alaskan Subarctic Fjords. In Estuarine Transport Processes, B. Kjerfve, ed., Univ. of So. Carolina Press, Columbia, S. C.

Nelson, C. S. (1977): Wind stress and wind stress curl over the California current. NOAA Tech. Rep. NWFS SSRF-714, Washington, D.C., 87 pp.

Officer, C. B. (1976): Physical Oceanography of Estuaries and Associated Coastal Waters. Wiley, New York, 465 pp.

Overland, J. E., M. H. Hitchman, and Y.-J. Han (1979): A regional surface wind model for mountainous coastal areas. NOAA Tech. Rep. ERL 407-PMEL 32, 34 pp.

Parker, B. B. (1977): Tidal hydrodynamics in the Strait of Juan de Fuca-Strait of Georgia. NOAA Tech. Rep. NOS 69, Washington, D.C., 56 pp.

Pashinski, D. J., and R. L. Charnell (1979): Recovery record for surface drift cards released in the Puget Sound-Strait of Juan De Fuca System during calendar years 1976-1977. NOAA Tech. Memo. ERL-PMEL 14, Washington, D.C., 30 pp.

Pease, C. H., R. J. Stewart, and J. E. Overland (1979): Report on FY-78 numerical modeling in the Strait of Juan de Fuca and Puget Sound. NOAA Tech. Memo. ERL-MESA 38, Washington, D.C., 32 pp.

Pritchard, D. W. (1967): What is an estuary: physical viewpoint. In Estuaries, G. H. Lauff, ed., AAAS, Washington, D.C., 3-5.

Rattray, M., Jr. (1967): Some aspects of the dynamics of circulation in fjords. In Estuaries, G. H. Lauff, ed., AAAS, Washington, D.C., 52-62.

Reed, T. R. (1931): Gap winds of the Strait of Juan de Fuca. Mon. Weather Rev. 59:373-376.

Saunders, P. M. (1976): Near-surface current measurements. Deep-Sea Res. 23:249-258.

Svendsen, H. (1977): A study of the circulation in a sill fjord on the west coast of Norway. Mar. Sci. Comm. 3:151-209.

Thomson, R. E. (1975): Currents in Juan de Fuca Strait: the physical oceanography of the B. C. coast--Part VII. Pacific Yachting, August, 84-91.

Wang, D.-P. (1979): Sub-tidal sea level variations in the Chesapeake Bay and relations to atmospheric forcing. J. Phys. Oceanogr. 9:413-421.

Wang, D.-P., and A. J. Elliott (1978): Non-tidal variability in the Chesapeake Bay and Potomac River: Evidence for non-local forcing. J. Phys. Oceanogr. 8:225-232.

Webster, I. (1977): A physical oceanographic study of Haro Strait: a data summary and preliminary analysis. Contractor rep. series 77-3, IOS, Patricia Bay, Victoria, B.C., 90 pp.

Weisberg, R. H., and W. Sturges (1976): Velocity observations in the West Passage of Narragansett Bay: A partially mixed estuary. J. Phys. Oceanogr. 6:345-354.